DOCTORAL DISSERTATION

Long-term and high-frequency streamflow variations in a shallow gravel-bed river
[浅い礫床河川における河川流量の長期および短期変動に関する研究]

September 2018

Department of Civil and Environmental Engineering

Graduate School of Engineering

Hiroshima University

AL SAWAF, MOHAMAD BASEL

Acknowledgements

The members of my supervisory committee deserve the best accolades and my deepest thanks for their expertise, encouragement and support. Dr. Kawanisi was particularly generous with his encouragement, as well as with opportunities for funding during the course of my academic career at the Hiroshima University. I would like to thank both Dr. Kaneko and Dr. Ghoda of Hiroshima University/Aqua Environmental Monitoring Limited Liability Partnership (AEM-LLP) for their unwavering technical assistance. Also, Dr. Shinya Nakashita is greatly appreciated. In addition, my friend Dr. Masoud Bahreinimotlagh for his willingness to help and support me within my study, I will never forget our golden days that we spent together in Hiroshima. Dr. Mochammad Meddy Danial was also a motivator during my study. Also, a special thanks to John Mensing not only for his language reviewing for my works but also for his insightful directions either in academia or in my life here in Japan.

Heartfelt thanks also go to my family, especially my parents, deserve a huge thankyou, for supporting my efforts to make something better of myself. I am grateful to all my friends that joined my life here at Hiroshima.

Mohamad Basel AL SAWAF
Hiroshima, Japan

Table of Contents

List of Symbols

Symbol		Unit
A	Cross-sectional Area along transmission line	m^2
H	Water Level	m
L	Horizontal distance between the transducers	m
Q	Discharge	m^3/s
h_m	Mean bottom elevation	m
A_B	Function of cross section bathymetry	m^2
u_m	Mean velocity through the sound ray path	m/s
θ	Angle between the ray path and the stream line	°
Z_B	Elevation of the riverbed along the transmission line	m
δQ	Discharge Error	m^3/s
δh_m	Water depth Error	m
δA_B	River bathymetry Error	m^2
δu_m	Water velocity Error	m/s
$\delta \theta$	Error the angle between the transmission line and the stream axis	°
t_{up}	Arrival time at upstream station	sec
t_{down}	Arrival time at downstream station	sec
WL	Water level	m
WS	Water Slope	m
T	Turbidity	FTU/NTU
SSC	Suspended Sediment Concentration	g/l

List of Notations

Notations	
ADCP	Acoustic Doppler Current Profiler
AVM	Acoustic Velocity Meter
CSA	Continuous Slope Area
CATS	Coastal Acoustic Tomography System
FATS	Fluvial Acoustic Tomography System
OAT	Ocean Acoustic Tomography
DF	Dam Flush
DFA	Detrended Fluctuation Analysis
RC	Rating Curves

List of Figures

List of Tables

Abstract

The landscape of the mountainous region of Hiroshima prefecture is unique in Japan. It provides opportunities for the development of run-of- river numerous projects. To design these kinds of projects effectively, long-term streamflow records are necessary. However, in order to assess the dynamics of rivers, a reliable characterization of river streamflow during unsteady flow regimes is of paramount importance. Measuring stage is one of the most common methods practiced at permanent gauging stations. Stage records are subsequently transformed to discharge by means of an estimated stage-discharge relationship, referred to as the Rating Curve (RC) method. To the best of my knowledge, there is currently no accepted approach to estimating discharge uncertainties. An empirical one-to-one relationship between water level and discharge evaluated from RC is determined under the important assumption that streamflow is steady, therefore, this method may be not precise in the case of streams that are subjected to unsteady flows. On the other hand, the development of various techniques and instruments has led to improved streamflow measurements. Among them, the Fluvial Acoustic Tomography System (FATS) that has been developed recently by Hiroshima University is proven to be able to manage various hydrological issues and problems and can be considered a promising technology in the field of water resources. In this context, this thesis focuses on the high-frequency and long-term monitoring of streamflow variations in the Gono River which is a shallow gravel-bed river located in the mountainous region of the Miyoshi-city of Hiroshima, Japan. This work is divided into three themes: (i) scaling characteristics of mountainous river flow fluctuations determined using a shallow-water acoustic tomography system, (ii) high-frequency acoustic monitoring of streamflow-turbidity dynamics in a gravel-bed river during artificial dam flush, and (iii) monitoring of streamflow-stage hysteresis behavior of a gravel-bed river.

The aim of the first theme is to investigate the scaling exponent properties of a mountainous river flow fluctuations by means of the Detrended Fluctuation Analysis (DFA) approach. Streamflow data were collected continuously using FATS, the results revealed that river discharge fluctuations have two scaling regimes and a scaling break. In contrast to the RC method, the small-scale exponent detected by the FATS

is estimated to be $1.02 \pm 0.42\%$ less than that estimated by RC. More importantly, the crossover times evaluated from the FATS delayed approximately by 42 ± 21 hr ≈ 2–3 days than their counterparts estimated by RC. The power spectral density analysis assists these findings. It is found that scaling characteristics information evaluated for a river using flux data obtained by RC approach might not be accurately detected, since this classical method assumes that flow in river is steady and depends on constructing a relationship between discharge and water level, while the discharge obtained by the FATS decomposes velocity and depth into two ratings according to the continuity equation. Hence, this work revealed the performance of FATS as a powerful and effective approach for continuous streamflow measurements at high-frequency levels.

The findings of the first project gave motivations to investigate the characteristics of turbidity–discharge (T–Q) dynamics corresponding to annual artificial dam flush release in a mountainous stream. Two methods for evaluating discharge were used in this study: the classical RC and the FATS. Interestingly, during dam flush, the discharge records obtained by the FATS showed striking features of unsteady streamflow behavior such as *discharge shoulders* and, in some events, *secondary discharge peaks*. According to the T–Q hysteresis loops, two types of T–Q pattern were observed: anticlockwise, which is the most common type, and figure-of-eight loops. Although the observed location was relatively far from the dam flush points, the primary reason for the anticlockwise hysteresis seemed to be soil erosion and scouring during flushing process across the river pathway being transported from the relatively long distance between the sediment sources and observation site.

Thirdly, the presence of the discharge shoulders as well as the secondary discharge peaks pushed us to monitor the unsteady behavior of streamflow, as well as, loops of streamflow-stage in this river. In order to determine river discharge, two methods were used: (i) the continuous slope area method (CSA), and (ii) the FATS. The findings showed that during a single hydrological event, the temporal variations in water slope has two peaks, and water slope-stage has a positive hysteresis behavior. In addition, streamflow-stage hysteresis loops estimated by FATS are informative more than streamflow-stages estimated by the CSA

method. Additionally, it was confirmed that streamflow-stage hysteresis loop increases with large-scale rainfall events. Finally, since it was found that streamflow-stage hysteresis loops estimated by FATS are informative, additional observation were included to present and to discuss the author's field investigation program during which a FATS was deployed to monitor and to observe streamflow-stage hysteresis in a mountainous shallow river, and the corresponding water slope-stage hysteresis loops as well. The filed program reports the unsteady behavior of streamflow in a moderate mountainous watershed during different scales of rainfall events and shed light the connection between of the streamflow-water level loops with surface slope-water level dynamics for a full fiscal year of different seasons.

CHAPTER 1: Background and purpose

1.1 Study Overview

Our earth is governed by well-defined seasonal periodicity, nonetheless, this climate system shows complex behavior, since it directly subjected to several and variable perturbations that can lead to extreme climate events [1]. Typhoons, Tsunamis, floods, and others are major natural disasters in Japan. Therefore, understanding the underlying issues that control the properties of both climate and hydrological systems is a paramount of importance.

Likewise, studying the dynamics of suspended sediment (SS) is necessary to further our understanding about drainage watershed processes and so make stronger and better management plans. Characteristics of a river catchment such as its geology, water drainage, slope, and land use are all features controlling the quantity and form of sediment mobilized into rivers [2–4]. Accordingly, there is a challenge to locate the sources of sediment and/or the causes of a watershed erosion and sediment storage are going on. Similarly, evaluation and determination of the contribution of streambank erosion to a basin budget is required in mitigating soil erosion and in introducing suitable protection and management practices to minimize stream SS and accompanying pollutant load [5,6].

Kawanisi et al. [7–9] launched a long-term project to measure the discharge in the Gono River by means of a novel hydroacoustic system called Fluvial Acoustic Tomography System (FATS). This system can measure the streamflow with high-frequency rates. However, they reported that the streamflow recorded by FATS changes at time scales of few tens of minutes to days [9]. This phenomenon in particular motivated the author to inspect the issues and the reason for these fluctuations what are their nature, characteristics, associated parameters, what are the reasons behind these fluctuations, etc.

Accordingly, the overreaching goal of this thesis is to address the issues subjected to long-term and high-frequency streamflow variations in a shallow gravel-bed river in Japan focusing on three fundamental themes: (i) the temporal scaling characteristics of the river flux observed by FATS and understand the nature of these fluctuation and their properties for high-frequency discharge records mainly by detrended

fluctuation analysis (DFA) approach, (ii) high-frequency hydroacoustic monitoring of streamflow-turbidity dynamics in during artificial dam flush events, and (iii) monitor the unsteady behavior of streamflow.

1.2 Objectives and motivations

The fundamental goal of this research is to investigate the underlying issues subjected to long-term and high-frequency streamflow variations mainly by means of a novel hydroacoustic tomography system and compare the new estimates to other current and common methodologies used for continuous monitoring of discharges in unsteady shallow gravel-bed stream. Field observations of this dissertation were conducted in the Gono River, which is a shallow gravel-bed river located in the city of Miyoshi, Japan. The scaling exponent characteristics of the Gono River discharge fluctuations by means of the detrended fluctuation analysis (DFA) method.

One of the important findings of the above project showed that the streamflow measured by FATS showed distinct temporal scaling on short time scales up to roughly 10 h compared with the corresponding discharge time series estimated by the RC method. This result inspired the author to go forward making a second study and to observe the variations of the streamflow behavior over high-frequency scales (i.e., short time periods of several hours) specifically within artificial dam flush events, and also to examine the relationship of the turbidity (T) and discharge (Q): (T–Q) hysteretic behavior related to lag time between peaks of discharge and turbidity. Therefore, the main aims of the second work are (i) to show up the properties of T–Q dynamics resulting from artificially operated dam flush, and (ii) to explore what information can be understood and observed from streamflow records obtained by FATS compared with discharges measured by means of the RC method.

Of interest, during dam flush, the discharge records obtained by the FATS showed striking features of unsteady streamflow behaviors. These behaviors gave the motivation to monitor the unsteady performance of streamflow, as well as, hysteresis in streamflow-stage in the Gono River for different scales of rainfall events.

1.3 Study site and state-of-the-art

1.3.1 Study area

The Gono River catchment area is 3900 km^2 located in the Miyoshi city of Hiroshima prefecture, Japan. The Gono River is a shallow gravel-bed river with a Manning roughness of approximately 0.03 estimated from the water surface profile and a bed slope of 0.11% around the observation site. The water depth at the observation location becomes considerably shallow under conditions of low flow. The grain-size distribution at the monitoring location reveals an average median size (d_{50}) of 27 mm and an average (d_{90}) of 115 mm. The grain-size distribution shows a lack of silt, fine sand, and clay [7]. The weather of Miyoshi is temperate, with annual average temperatures varying from 8.5°C to 19.4°C and a mean yearly precipitation of 1492 mm. The river is 115 m wide The Saijo River and the Basen River are the main tributaries of the Gono River, unite 2.7 km upstream of the observation site, and the confluent rivers meet the Gono River 0.9 km downstream of the junction (Fig. 1.1). The annual mean flowrate at the Ozekiyama gauging station (the nearest station to our experiment site), located approximately 1.1 km upstream of the study site, is estimated to be approximately 75 m^3/s (see Fig. 1.1(a)). The locations of the experiment site and the FATS transducers (T1 & T2) are shown in (Fig. 1.1(b)).

The Gono River is the habitat of the Ayu and Yamame sweetfish, which feed on sphagnum growing on bedrock in the Gono River streams. Therefore, according to the framework of the Ministry of Land, Infrastructure, Transport, and Tourism (MLIT) of Japan, to protect and promote fishery resources in the Gono River, water from both Haji and Haizuka dams is scheduled for flushing ordinarily once a year at the end of March [8]. The Haizuka dam, is built around 26 km upstream from the study area whereas the Haji dam, which is located around 40.2 km upstream from the experiment site.
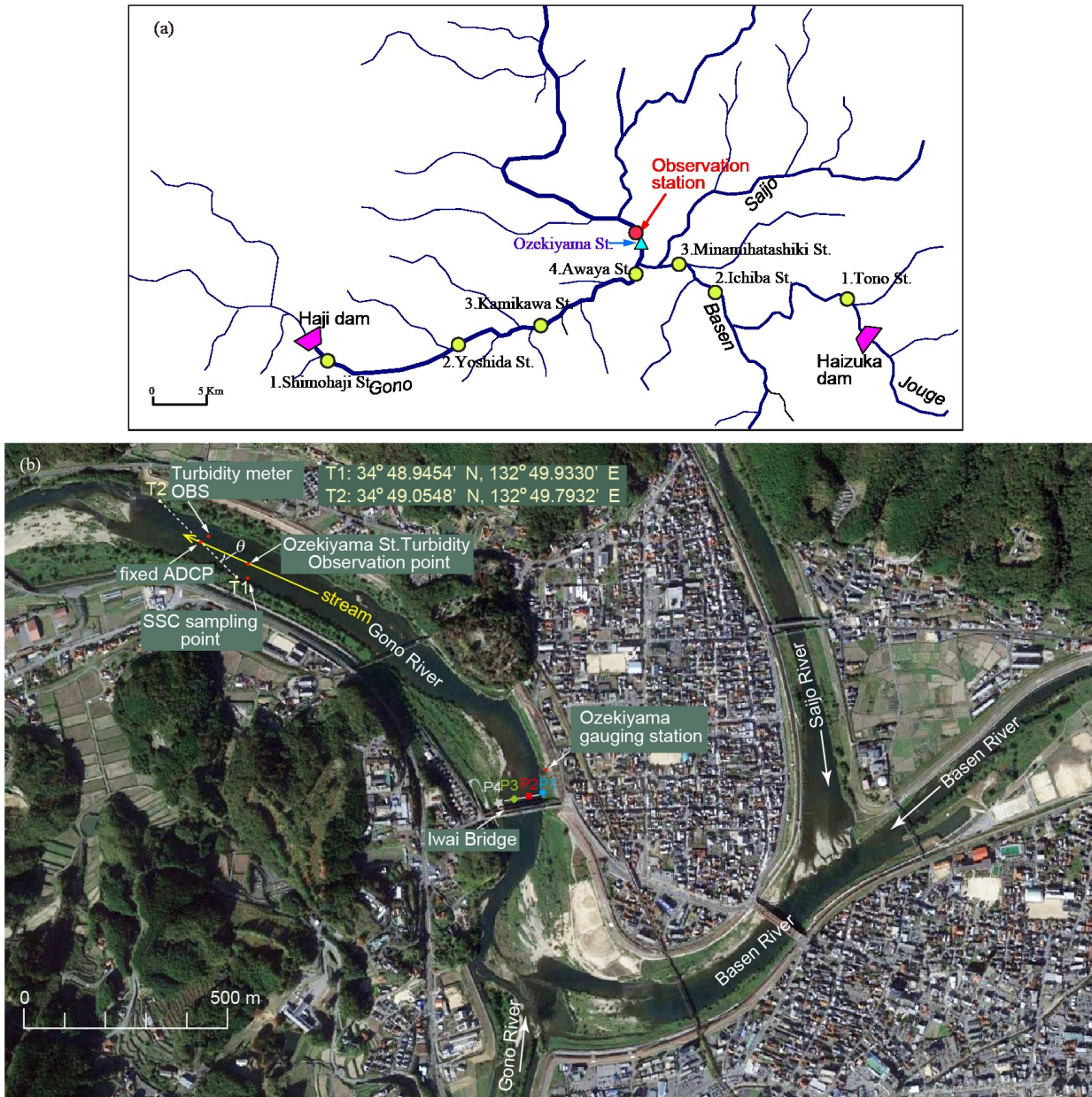
Figure 1.1 (a) The Gono River and places of Haji and Haizuka dams. (b) Position of field measurement site and locations of installed FATS, turbidity snode (OBS), and fixed ADCP, (P1, P2, P3, P4) are the monitoring points of the Rinko profiler for turbidity observations.

Upstream of the monitoring site and the Ozekiyama gauging station, there are four gauging stations that measure hourly water level alongside the river branch that takes water from the Haji dam. This enables us to evaluate the discharge there using the RC approach based on their specific site conditions. On the other

side, only three gauging stations are distributed alongside the river branch that receives the released water from the Haizuka dam (Fig. 1.1(a)).

1.3.2 Fluvial Acoustic Tomography System (FATS)

1.3.2.1 System description

Acoustic tomography systems are efficient hydroacoustic systems in estimating several water properties such as current velocity, temperature, salinity, discharge, etc. Initially, the Ocean Acoustic Tomography (OAT) was designed to measure mesoscale ocean currents employing high-powered signals with transmission frequencies less than 1kHz [10,11]. Kaneko et al., [12] developed a new measuring acoustic tomography system that apply the operational methodology of OAT called Coastal Acoustic Tomography System (CATS) to map the temperature variations in the Sea of Japan. Further improvements allowed precise transit time measurements which led to the successful flow mapping in coastal waters [13].

Unlike OAT, CATS employs acoustic signals at frequencies up to 10 kHz this range of frequencies are important to overcome the small water areas (i.e. coastal scales) and hence to improve both receiving and transmission proficiency. Yet, the transmitted frequencies employed by CATS are considered as high-power signals thus the measured sound travel time between two acoustic stations separated from each other are in orders of kilometers in waters depths less than 10 m. The key reason behind the FATS is to improving the applications of acoustic system developed by Kaneko et al. [12] to even shallower waters. However, Razaz et al. [14] examined shallower flows varying from mountainous streams (0.5 m deep) to the mouth of estuaries in coastal areas (maximum 10 m deep).

The principle of FATS is based on the "time-of-travel" approach, such as using acoustic velocity meters [15]. Though, the acoustic signals of FATS are emitted from omnidirectional transducers in the range of 10–55 kHz. Unlike other approaches, cross-sectional average velocity can be measured by FATS with no additional for any complicated post-processing steps [7].

FATS is supported by Global Positioning System (GPS) receivers (u-blox LEA-6T), thus the satellite information from those receivers enable a high-precision standard frequency (10 MHz) and precise timing

pulse (1 Hz), which are necessary to guarantee and maintain that both upstream and downstream systems run exactly concurrently. The 10-MHz signal is used as the base clock of FATS system for high-precision processing of the transmitting/receiving signal. Every 30 s, acoustic beats are triggered by a GPS clock and are transmitted simultaneously from two transducers installed across the river banks diagonally. Fig. 1.2 illustrates the installation and operation process for the FATS in river.
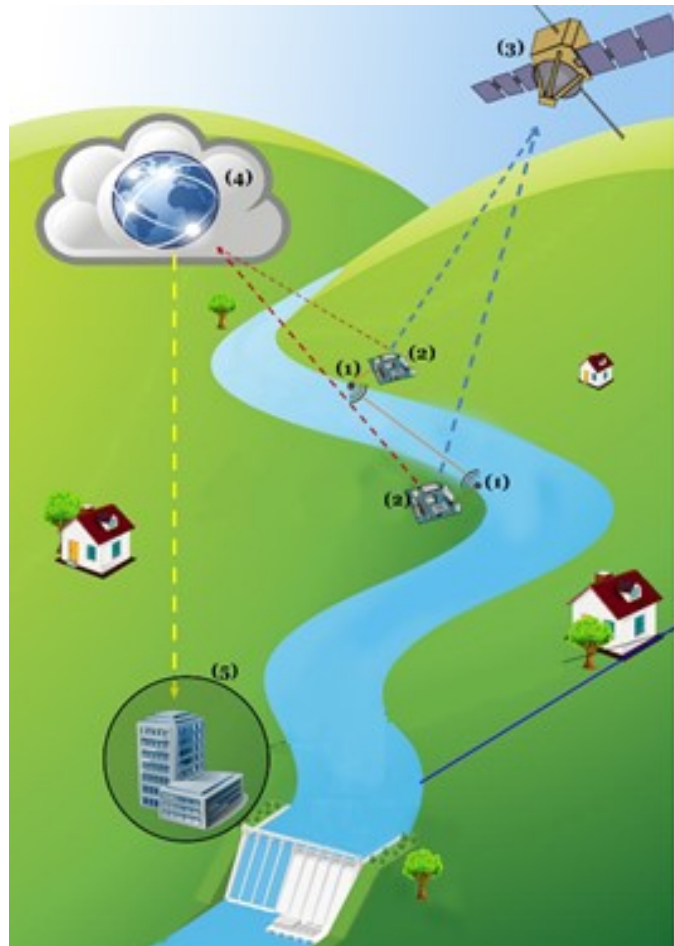
Figure 1.2 Schematic representation of the FATS and its operation in river.

Since the FATS utilizes travel-time tomography approach, the arrival time of acoustic signals at the upstream (t_{up}) and downstream stations (t_{down}) (see Fig.1.2), the sound speed (c) and streamflow velocity along the sound ray path (u) are determinable according to the following equations:

$$c = \frac{L}{t_m} \tag{2.1}$$

$$u = \frac{c^2}{2L} \Delta t \tag{2.2}$$

where L is the horizontal distance between the upstream and downstream transducers, $t_m = \frac{t_{up}+t_{down}}{2}$ and

$\Delta t = t_{up} - t_{down}$.

Field observations by means of FATS were conducted at the location designated in (Fig. 1.1). A couple of omnidirectional broadband transducers (T1 and T2) were installed diagonally across the river, the deployment of the transducers is shown in (Fig. 1.1(b)). The length of the transmission line between the pair of transducer was roughly $295 \pm 1\text{m}$ (varied within the years of measurement campaigns). The acoustic pulses (central frequency: 30 kHz) were transmitted concurrently from both transducers every 30 s. Also, the acoustic pulse was modulated by a single 9th order M-sequence.

The streamflow Q by means of FATS is given as:

$$Q = (H_m - z_{Bm})L \tan\theta \times u_m \tag{2.3}$$

where L= length of the transmission line; H_m = arithmetical mean of both water levels; u_m = section-averaged velocity along the acoustic path; θ = flow angle; and z_{Bm} = mean bed level along the transmission line can be estimated according to the below equation:

$$z_{Bm} = \frac{1}{L}\int_0^L z_B(y)dy \tag{2.4}$$

For clarification, river cross-section during observation site is shown in (Fig. 1.3) The cross-path configuration can be used to determine the streamflow angle θ can be measured as demonstrated [8,16], however, in our observations the flow direction angle θ was measured using a moving-boat ADCP [7,17]. Recently, Kawanisi et al. [18] estimated the parameters z_{Bm} and θ using the discharge data from RCs assuming that the parameters were constant for the 1-month duration. Also, in the present study, the bed

level z_{Bm} between both transducers was directly measured using moving-boat ADCP and in some circumstances a single-beam echo sounder and updated periodically (each 4 to 6-month intervals).
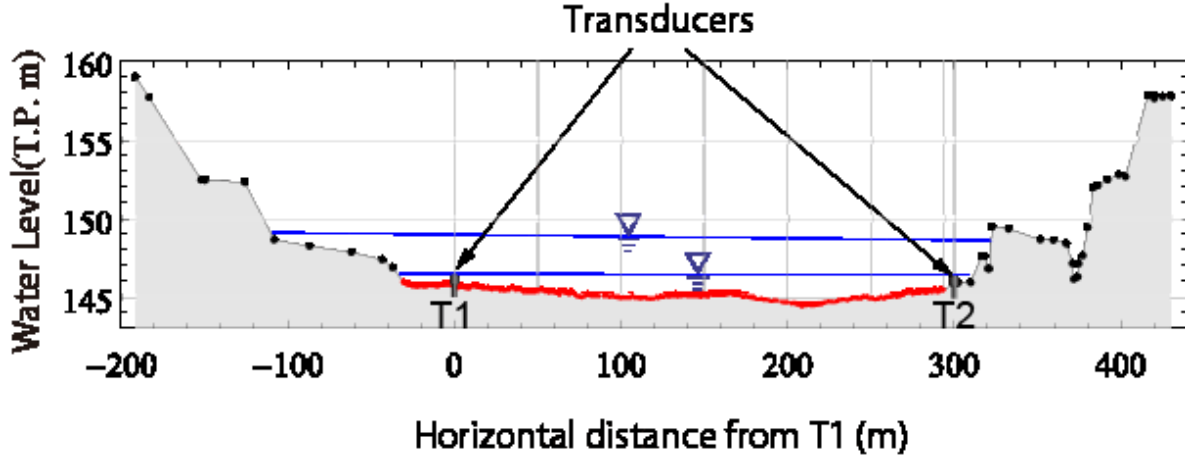
Figure 1.3 River cross-section at the observation location and the places of Transducers T1, T2.

1.3.2.2 Error structure in discharge measurement by the FATS

Kawanisi et al., [9] had fully studied the error structure affecting FATS discharge measurements. These errors include:

(i) river-bed bathymetry,

(ii) cross-sectional average velocity along the transmission line between the acoustic transducers,

(iii) direction of the streamflow angle between the transmission line and the stream axis, and

(iv) water depth. The errors effecting on Q are expressed as:

$$\delta Q = \delta Q_{h_m} + \delta Q_{A_B} + \delta Q_{u_m} + \delta Q_\theta$$

$$= \frac{\partial Q}{\partial h_m} \delta h_m + \frac{\partial Q}{\partial A_B} \delta A_B + \frac{\partial Q}{\partial u_m} \delta u_m + \frac{\partial Q}{\partial \theta} \delta\theta \tag{2.5}$$

Therefore, the relative error of streamflow (Q) can be written as:

$$\frac{\delta Q}{Q} = \frac{\delta Q_{h_m}}{Q} + \frac{\delta Q_{A_B}}{Q} + \frac{\delta Q_{u_m}}{Q} + \frac{\delta Q_\theta}{Q}$$

$$= \frac{\delta h_m / h_m}{1 - A_B/(L h_m)} + \frac{\delta A_B / A_B}{1 - L\, h_m/(A_B)} + \frac{\delta u_m}{u_m} + \frac{\delta\theta}{\cos\theta\,\sin\theta} \tag{2.6}$$

24

The relative error for the river water depth $\frac{\delta Q_{hm}}{Q}$ is equal to δh_m relative to the mean water depth, i.e. Mean-depth = h_m -A_B/L. Thus, for shallow streams, correct river depth estimations are important. Regarding the second error term ($\frac{\delta Q_{A_B}}{Q}$) is influenced by the quality of bathymetric mapping campaign and temporal variations in the bottom topography. Since the uncertainty of the velocity obtained by FATS is independent of the velocity magnitude [7], low flows enhances the relative error. The uncertainty of the streamflow direction can potentially induce substantial error in the case of a small value of θ [7].

Figure 1.4 Plan view for the river bathymetry around observation site (height above mean sea level), and the places of Transducers T1, T2.

CHAPTER 2: Scaling characteristics of mountainous river flow fluctuations determined using a shallow-water acoustic tomography system

2.1 Introduction and purpose

Well-defined seasonal periodicity governs our climate system, nonetheless, our climate system has a complex behavior, since it directly subjected to several and variable perturbations that can lead to extreme climate events [1]. Therefore, additional information is required to recognize the underlying issues that govern and control the properties of both hydrological and climate systems. To establish reliable evaluations, hydrological models need precise river discharge data. This also encompasses using robust and reliable measurement approaches.

Numerous studies have examined the streamflow scaling characteristics by means of various methods [19–25]. These works have investigated the long-memory and multifractal characteristics of river streamflow for quite a lot of rivers in the world. Nevertheless, the relationship between these properties and the physical processes that control the river flow is still not imperfectly understood [24].

Tessier et al. [19] examined the daily river discharge from 30 various watersheds in France with drainage areas of 40–200 km^2. They reported that river flow fluctuations have two scaling regimes, one for time scales shorter than 16 days and the other for time scales exceeding 16 days. Pandey et al. [20] analyzed the daily river flows from 19 several river basin in the US with drainage areas varying from 5 to 1.8×10^6 km^2; their results showed a scale break at about one week and no dependence of the multifractal parameters on catchment surface. Zhou et al. [21] investigated the multifractal scaling behavior of long-term records of daily runoff time-series in 32 subwatersheds of different watershed areas in the US ranging from 0.01 to 333.8 km^2; they reported a scale break at 6 days for some watersheds and no scale break for the other watersheds.

The relationships between basin areas and long memory was studied by Mudelsee [26] by using river flow

records of several stations distributed in six river basins in America, Europe, and Africa. He stated that larger watersheds have stronger memory.

Furthermore, Hirpa et al. [24] performed a detailed river flow fluctuation analysis of daily records from 14 different stations in the Flint River Basin in the US with basin sizes varying from 23 to 19,606 km^2. They concluded that river flow fluctuations have two scaling regimes and crossover times that varied from 1 to 20 days and increased with the increase in watershed area. Moreover, they concluded that the long memory of river flow fluctuations does not come from long memory of the corresponding rainfall.

In terms of river characteristics, Labat et al. [27] studied the discharge fluctuations of two karstic catchments in France. They reported that karstic flow fluctuations have three distinct temporal scales: the first scale ranged from 1 h to around 100 h, the second scale ranged from around 100 h up to 1 year and the third scale ranged for more than 1 year.

Livina et al. [25] utilized the DFA method to study the temporal scaling characteristics of the discharge of three Bavarian rivers by using two flux time-series (a real discharge record and a corresponding ASGi model record). They stated that river flow records are highly short-term correlated and less correlated in the asymptotic range. Additionally, in most cases, the results of ASGi model described the real basin processes adequately.

Kawanisi et al. [7–9] launched a long-term project to measure the discharge in the Gono River by means of a novel hydroacoustic system called Fluvial Acoustic Tomography System (FATS). This system can measure the streamflow with high-frequency rates. However, they reported that the streamflow recorded by FATS changes at time scales of few tens of minutes to days [9]. This phenomenon motivated us to study the temporal scaling characteristics of the river flux observed by FATS and understand the fluctuation properties of high-frequency signal discharge records mainly by detrended fluctuation analysis (DFA).

2.2 Study site and data description

Field observations using FATS were carried out at the location designated in (Fig. 1.1) and described in section 2.1. River discharge in this study was continuously measured using the FATS in the Gono River,

and the observation period for our study started from 1st December 2015, to the end of May 2016. The time resolution of discharge estimated by FATS was 10 min. A reference for the discharge data collected by FATS, the available hourly streamflow records observed by Ozekiyama gauging station (Fig. 1.1) for the same study period were utilized in our work. Discharge in Ozekiyama gauging station is generally estimated based on river stage measurements through well-established Rating Curve equations (RC) that are defined by the Ministry of Land, Infrastructure, Transport and Tourism (MLIT), Japan.

2.3 Detrended fluctuation analysis

Peng et al. [28], proposed the Detrended Fluctuation Analysis (DFA) approach, which is a scaling method used to determine the long-range power correlation exponent in noisy signals. In this research, the DFA is employed to detect the long-range correlation in non-stationary time-series with trends since, it is a recommended approach to study the streamflow fluctuations in rivers compared to the power-spectral-analysis method where stationarity is required [23,28–30]. The DFA can be accomplished according to the following steps:

1- Identify and eliminate the periodicity from the discharge time-series, this is necessary since river discharge fluctuations are greatly influenced by the seasonal climate variations that otherwise could be confused with long-term correlation. In the case of this thesis, the mean interannual periodic seasonality was detected from the available hourly discharge data records provided by the MLIT, from 2002 to 2016, and thus, the seasonality was eliminated following the same approach described by JanW. Kantelhardt et al. [31] i.e., subtracting the mean over different years of each calendar day $\bar{Q}(i)$ from the record $Q(i)$. The mean $\bar{Q}(i)$ is calculated for each calendar date i, (e.g., 1st of March, by averaging all years in the record from (2002 to 2016)) as follows:

$$B_t(\text{i})= Q(i) - \bar{Q} \text{ , for } i=1, 2,..., n$$

(2.1)

where $B_t(i)$ represents the residual sum of the fluctuation and trend components. Next, a profile $y(k)$ is created by generating the cumulative sum for the time-series $B_t(i)$ according to the following formula:

$$y(k)= \textstyle\sum_{i=1}^{k} B_t(i) \;\;, \; k= 1,2,...,n \tag{2.2}$$

2- After determination of the profile $y(k)$, the author split it into segments of identical length n and find the polynomial approximation p_n using least squares fit in each segment separately, representing the trend in each section.

Linear, quadratic, or even higher order polynomial fit can be applied for the fitting process, leading to the so-called DFA1, DFA2, and DFA3, etc. However, the application of first-order DFA1 may yield higher correlation exponents that lead to an inaccurate estimation of the long-term persistence [31]. Furthermore, DFA1 is not informative in the case of analysis of such nonlinear and highly non-stationary data as river discharge, and because the author is interested here with investigating fluctuations of river discharge with high-frequency rates, DFA2 and DFA3 were applied in our study.

3- The average fluctuation $F(n)$ of the signal around the trend is given by the following formula:

$$F(n) = \sqrt{\frac{1}{N}\sum_{k=1}^{N}(y(k) - p_n(k))^2} \tag{2.3}$$

4- This calculation is repeated over all time scales (box sizes) to characterize the relationship between $F(n)$, the average fluctuation, and the box size n. As a general case, $F(n)$ increases with box size. A linear relationship on a log–log plot indicates the existence of power law (fractal) scaling. Under such conditions, the fluctuations can be characterized by a scaling exponent α, corresponding to the slope of the line relating log $F(n)$ to $log(n)$ [28], The slope α of the line $F(n)$–(n) determines the scaling exponent:

$$F(n) \approx n^{\alpha} \tag{2.4}$$

5- The scaling exponent α (scaling exponent, autocorrelation exponent) describes the behavior of time-series as:

   i. $0 < \alpha < 0.5$ indicates anti-correlated signal

   ii. $\alpha = 0.5$ indicates white noise

   iii. $0.5 < \alpha < 1$ indicates correlated time series

iv. $\alpha = 1$ indicates $1/f$ pink noise, and
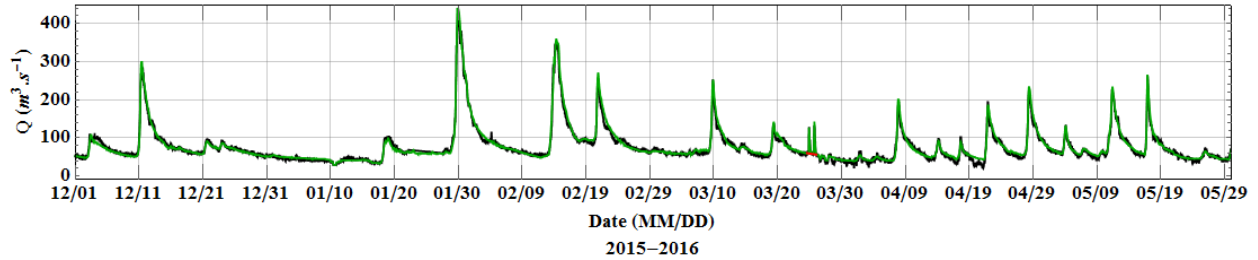
Figure 2.1 Streamflow time-series during the study period for estimated by: RC (Green), FATS (Black).

v. $1 < \alpha < 1.5$ indicates random walk and $\alpha \sim 1.5$ corresponds to Brownian noise.

2.4 Results and discussion

2.4.1   Scaling-exponent characteristics

The basic goal of this work is to explore the vague issues that is subjected to discharge fluctuations which occur in the very short-time periods captured by FATS. Kawanisi et al. [7,9] reported that the discharge time-series records obtained by means of the FATS exhibit an interesting phenomenon, which is the diurnal fluctuations of river flow in short term, i.e., (daily &sub-daily) fluctuations that cannot be detected by the classical measurement approaches.

The discharge time-series during the study period for both FATS and RC is shown in (Fig.2.1). This figure presents that streamflow time-series estimated by the RC approach has a smooth behavior compared to the discharge time-series determined by FATS. Revealed in (Fig. 2.2) a larger window proves the existence of streamflow variations between FATS and RC that take place in the short-time periods. This figure displays the performance of FATS in detecting the high-frequency oscillations continuously measured in river discharge that happen in very short time scales and cannot be observed easily by other common systems. Regarding the DFA analysis, the author first applied the DFA approach for discharge data to evaluate the scaling exponents of river streamflow fluctuations. Fig.2.3 presents the DFA2 and DFA3 graphs for FATS

and RC discharge data over the observation period. The points of DFA on the log–log plot can be approximated by two lines:

The first line has a steep slope at short lag times, while the second line has a moderate slope at longer lag times, which apparently reveals the presence of two scaling regimes for the discharge time-series. A linear regression approximation fit was calculated to the two regimes separately, excluding the points that have substantial deviation from the sequence of the entire points and points adjacent to the crossover to obtain accurate results.

Accordingly, the least confidence interval selected for our study was 95% to calculate the DFA scaling exponents in our research. The intersection points of the two fitting lines procedure the crossover time that are revealed by the small vertical bars. It can be seen that the crossover time estimated by RC was about 75 hours, whereas it was estimated to be approximately 127 hours by FATS. The relatively large variance between the crossover time observed by RC and FATS motivated us to investigate more deeply about this variance. Thus, the author repeated the same analysis procedure by dividing the original observed time-series and studying two successive months, i.e., December 2015 & January 2016, January & February 2016, February & March 2016, March & April 2016, and April to May 2016. The purpose of this division and repetition is to examine the role of the external input flows (rainfall events and dam flush) on the scaling exponents and crossover time characteristics. Besides, the author aimed to investigate how short-term exponent characteristics vary over time.

Because the author observed that the crossover time occurred within around 4 days, the author increased the length of the partitioned time-series to 2 months instead of one month to make certain that the slope α is being correctly evaluated over the two regimes. Prior to the scaling-exponents results, it is important to comment on the discharge estimates within the studied period. The chart shown in Fig. 2.4 presents the average discharge value corresponding to each studied segment.
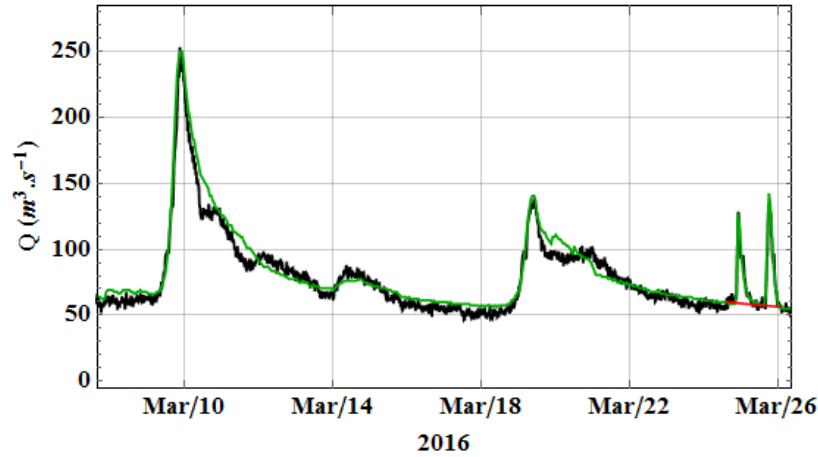
Figure 2.2 Demonstration for the FATS in detecting high-frequency variations (daily &sub-daily) of river discharge; RC (Green), FATS (Black), ARIMA model for forecasting baseflow within dam flush events (Red).

The flow rate calculated by both methods were nearly similar. Kawanisi et al.[9] discussed the uncertainties of discharge obtained by FATS in contrast to RC, and they proved that the relative difference between the 20-hr averaged Q_{FATS} estimate and the Q_{RC} does not exceed $\pm$ 6% for Q_{FATS} averaged for 20 h and discharge obtained by the FATS is reliable.

The outcomes of the high-frequency scaling exponents are presented in Table.2.1 The mean values for $\alpha1$ observed by FATS and RC were roughly 1.7 and 2.2, correspondingly. Obviously, $\alpha1$ exponents obtained by FATS are lower than their counterparts evaluated by RC. This may be justified due to the nature of the RC approach that shows a smooth discharge time-series. The mean difference between FATS and RC results is approximately 0.51±0.21, which corresponds to a difference equal to 1.02±0.42%. This difference may be of great importance for streams that have values approaching the limit of two adjacent characteristics of scaling exponents. Although the small DFA scale exponents resulted from FATS less than those that resulted from RC, both $\alpha1$outcomes indicated Brownian noise behavior for the fluctuations of the time-series in high-frequency scales. Large DFA-scale exponents that reveal the long-memory characteristics of the river flow fluctuations are presented in the same table. As shown in this table, the
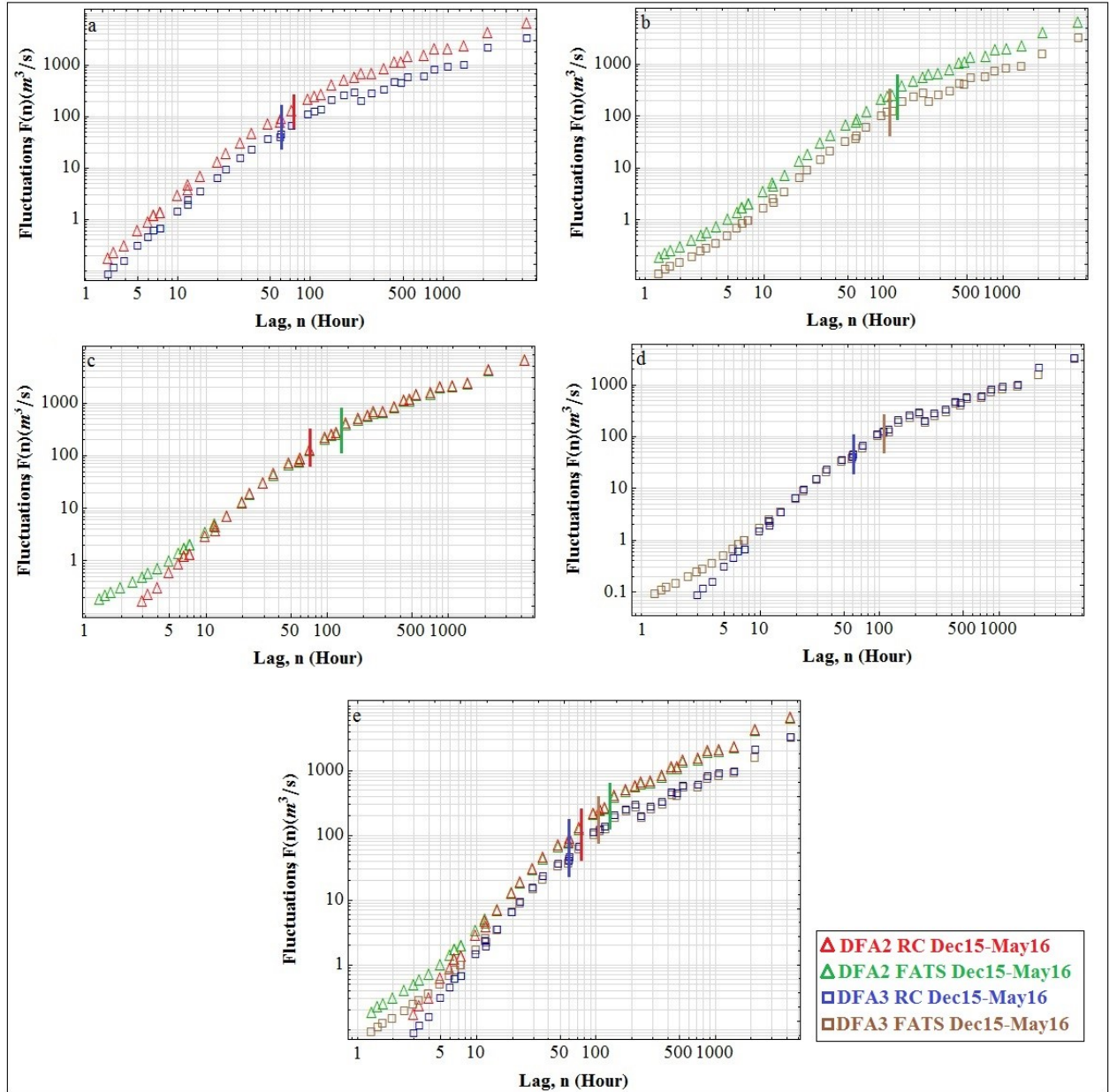
Figure 2.3 Detrended fluctuation analysis of orders 2 and 3 from December 1, 2015 to May 31, 2016); (a) RC approach pairwise comparison between DFA2 and DFA3 results, (b) FATS pairwise comparison between DFA2 and DFA3 results, (c) DFA2 pairwise comparison between RC and FATS results, (d) DFA3 pairwise comparison between RC and FATS results, and (e) overall comparison between DFA2 & DFA3 for RC and FATS.

values of $\alpha 2$ fluctuate around 0.92. This result proves that discharge time-series has persistent long-range power law correlations and confirms previous findings [19–21,23,24] that show river flow has long memory.

Table 2.1 Scaling exponent for both DFA2 and DFA3 for streamflow estimates determined by FATS and RC in each studied period.

Discharge period	DFA2						DFA3					
	RC			FATS			RC			FATS		
	α1	α2	Crossover time (hr)	α1	α2	Crossover time (hr)	α1	α2	Crossover time (hr)	α1	α2	Crossover time (hr)
Dec15 & Jan16	2.27	0.91	56	1.71	0.93	102	2.37	0.94	42	1.65	0.94	97
Jan16 & Feb16	2.22	0.93	88	1.75	0.94	151	2.25	0.90	65	1.73	0.91	128
Feb16 & Mar16	1.97	0.90	110	1.67	0.94	126	1.97	0.90	96	1.66	0.94	129
Mar16 & Apr16	2.05	0.91	68	1.67	0.91	90	2.09	0.91	48	1.68	0.93	83
Apr16 & May16	2.19	0.91	51	1.71	0.94	90	2.26	0.90	80	1.69	0.90	83
Dec15 & May16	2.17	0.91	75	1.67	0.92	138	2.22	0.92	60	1.68	0.88	112

Of interest, the results observed from the analysis of large-scale DFA exponents are reliable. That is to say, the values of $\alpha2$ for both discharge estimate approaches FATS and RC are approximately or even same in some periods in terms of DFA2 or DFA3. This result proves fluctuation properties detected by FATS is roughly similar with other classical measurement approaches. Thus, this finding supports the other works of Kawanisi, et al.[7–9,32] that proved the feasibility and high performance of automatic monitoring of streamflow at a high temporal resolution by the FATS.

The crossover times for our observation clearly indicates a delay in break time observed by FATS in contrast to RC by approximately 42±21 hours, this finding might be more significant in large catchments where their crossover times are high.

To verify the reliability of our results and confirm that only two scaling regimes exist for our studied river, the author calculated DFA2 scaling properties for the hourly data of Ozekiyama from January 2014 to the end of May 2016. The DFA2 analysis for this time-series resulted in $\alpha1=2.1$, $\alpha2=0.87$, and crossover time of around 2 days. These results seem to be in the range of the former findings. Thus, the values of $\alpha2$ in our study might be minimized from 0.92 to approximately ≈ 0.87 if the FATS time-series encompassed longer streamflow data of several years.
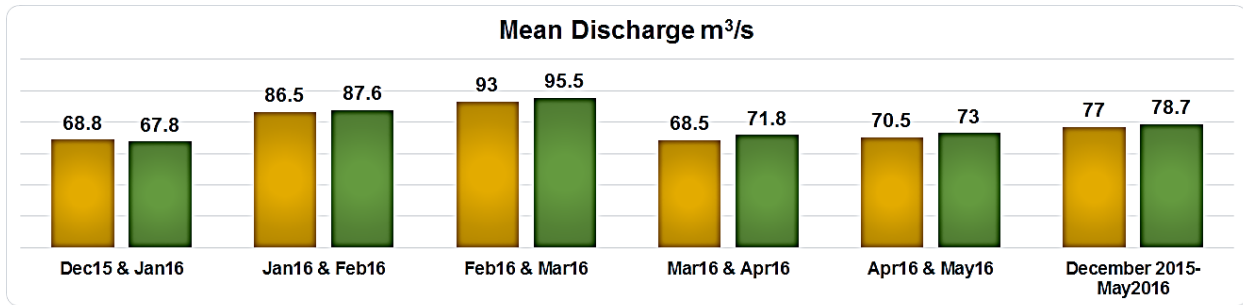
Figure 2.4 Mean flow rates estimates for both FATS (Yellow) and RC (Green) for each studied period.

2.4.2 Effects of external inputs to the river regime (flood events and dam flush) on crossover time

The outcomes in Table 2.1 indicate a variation in crossover times values within the studied periods. The crossover times fluctuated around a certain value. The question that arises is what kind of relationship existed between the crossover time and river discharge peak. To answer this question, the author focused on the peak characteristics of river discharge, and the discharge peaks are generated due to the intense rainfall events and the contribution of dam flush.
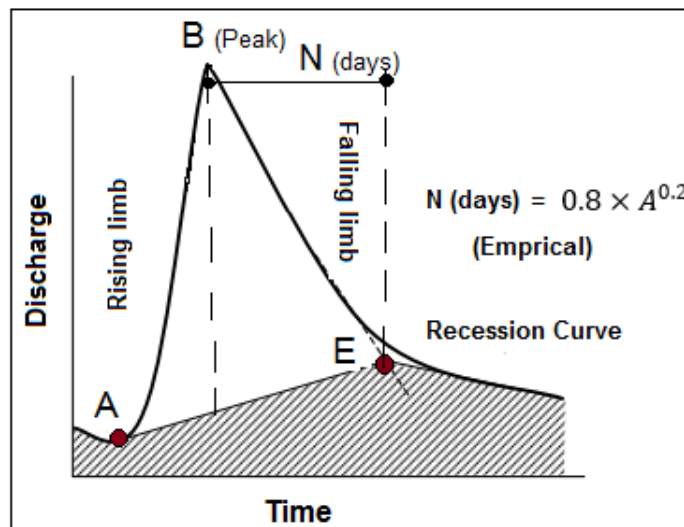
Figure 2.5 Direct runoff separation.

Table 2.2 Mean values of DFA2 and DFA3 results and the corresponding runoff intensity and duration for each studied period.

Discharge period	RC			FATS			Total Time for All Runoff Events (hr)	Total Runoff Discharge (m³/s)
	$\alpha1$	$\alpha2$	Crossover time	$\alpha1$	$\alpha2$	Crossover time		
Dec15 & Jan16	2.32	0.93	49	1.68	0.93	100	639	559
Jan16 & Feb16	2.24	0.92	77	1.74	0.93	140	470	657
Feb16 & Mar16	1.97	0.9	103	1.67	0.94	128	573	1188
Mar16 & Apr16	2.07	0.91	58	1.68	0.92	87	1012	1126
Apr16 & May16	2.23	0.91	66	1.7	0.92	86	1207	678

To explore the effect of rainfall events, all discharge waves produced by rainstorm events were separated completely into runoff flow and baseflow by a graphical approach of hydrograph separation [33], as illustrated in (Fig.2.5). The separation is achieved by matching a straight line from the hydrograph point of rise (A) to the inflection point (E) on the hydrograph, N days after the peak.

It must be mentioned for a couple of discharge peaks on the end of March were caused by flushes from Haji and Haizuka Dams (Fig. 1.1). To evaluate and separate the contribution of dam flushes, the author predicted an ARIMA model for the baseflow that corresponds to the dam flush events and eliminated the inputs of dam flushes (see Fig. 2.2).

Table 2.2 shows information about the average results of DFA2 and DFA3 for both discharge methods, total runoff discharge, and the corresponding total runoff time observed in each period. As shown in Table 2.2, crossover times observed by the RC method does not reveal clear information; instead, the findings show that break scales times observed by FATS are inversely proportional with the duration of runoff events. In other words, the crossover time delayed as the total time for runoff event decreased, which resulted from the runoff events and dam flush inputs.

The crossover times fluctuate around 3 to 5 days, bearing in mind the finding of Hirpa et al. [24], who proved that the scale break time occurs from 1 to 20 days and increases with the increase in the watershed area. Considering the relatively small area of our catchment area, the author concluded that the crossover

time is directly proportional to the watershed area; however, the duration of runoff events due to external inputs (flood and dam flush) might have minor impacts on the crossover time.

Genearlly speaking, the difference for the detected crossover time and the small scaling characteristics between the FATS and RC because of the approach. In other words, the discharge obtained by the FATS decomposes velocity and area into two ratings according to the continuity equation, instead of rating the stage component alone to construct a relationship between the discharge and the water level in the RC method. Thus, this study suggests that the scaling characerstic information of river discharge maybe missed by using flux data obtained by the RC method and can be adequatly detected by using FATS. Interestingly, Livina et al. [25] demonstrated that some statistical characteristics of river discharges using the ASGi model data are similar to real basin processes. Infact, incorporating discharge data of FATS with such competitive modeling systems helps to extent our knowledge on the hidden scaling properties in the river regimes. Therefore, this study suggests that additional invstigation is still required to improve the performance of the hydrological models.
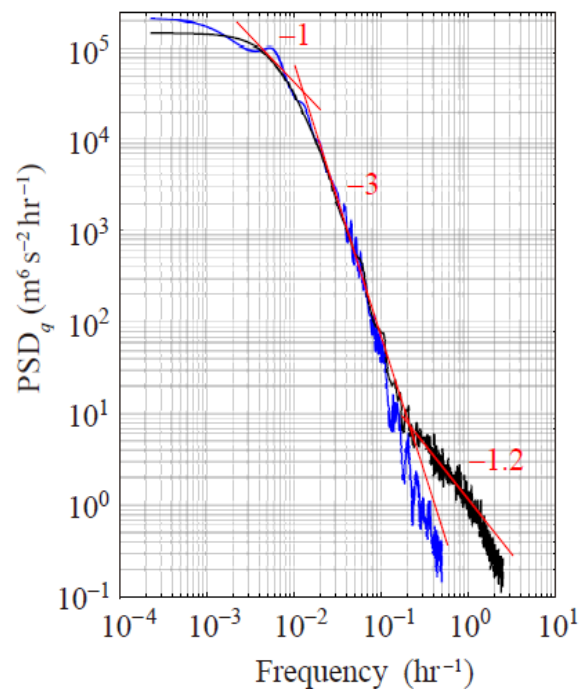
Figure 2.6 Power spectra of streamflow fluctuations for both RC (Blue) and FATS (Black) (December 1, 2015 to May 31, 2016).

2.4.3 Power spectral analysis

Dolgonosov et al.[34] introduced a model of river runoff power spectrum, in which all salient features of the basin area such as the structure of river network, the existence of lakes and dams, and rainfall characteristics, are included into the model parameters. The power spectrum is given as follows:

$$S(f) \propto \left(\frac{1}{f^\beta}\right)\left(\frac{1}{f_c^2 + f^2}\right) \qquad (2.5)$$

The runoff spectrum is the product of the precipitation power spectrum and the Lorentzian factor $\left(\frac{1}{f c^2 + f^2}\right)$ damping. The exponent β is approximately 1. If f is small compared to the crossover frequency f_c, $1/f$- noise specifies behavior of the spectrum, whereas when f passes through the point f_c, the Lorentzian transforms into f^{-2}, and after multiplication with $1/f^\beta$, it yields a trend of $1/f^{(\beta+2)}$ at high frequencies.

Fig 2.6 shows the power spectrum of discharge evaluated by FATS and RC approaches. The results of power spectral density show that the exponent value in the mid-frequency region is approximately 3. In contrast, the short-time scales are captured by the FATS, and for the present average length of 1 hour, the cutoff frequency is approximately 0.3 hr^{-1}; the discharge variations at this level are still under investigation. The crossover frequency f_c is observed around 1.35×10^{-2} hr^{-1} and corresponds to a period of 75 hr $\approx$ 3 days. The period is comparable to the crossover time detected by the DFA method. In addition, the crossover period may be proportional to L/u, where L represents the catchment length and u represents the mean flow velocity. Hence, the crossover period depends on the catchment length, the mean bed slope, and the intensity and period of the rainfall event. Thus, the break scales times for the Gono River is relatively small.

Finally, it can be said the high-frequency region detected by the FATS may attributed to the spatial variations of river discharge as the river roughness varies with stage.

2.5 Conclusions

This contribution, the DFA method used to investigate the scaling characteristics of river discharge fluctuations calculated by two methods: RC and FATS. Unlike the RC method, the results obtained by

FATS are more adequate, this because the discharge estimated by FATS decomposes velocity and depth into two ratings instead of rating the water level alone to discharge as accomplished in the RC approach and one drawback for the RC method is considering the discharge in river is steady.

Flow fluctuations in the Gono River are characterized by two scaling regimes: one at short time scales and the other at long time scales, and a crossover time is observed around 4-5 days. The DFA findings of finer scale $\alpha 1$ estimated by FATS were less than those estimated by RC by 1.02±0.42%; this outcome might be important for rivers that have values approaching the limit of two adjacent characteristics of scaling exponents. Further, the large DFA exponent $\alpha 2$ showed that the river flow fluctuations have long memory. In contradiction of RC method, FATS detected a crossover time lagged by 42±21 hours, which is not small and might indicate significant values for larger watershed. The detected crossover time is mainly a function of the watershed area, and the results indicated that crossover times observed by FATS are inversely proportional with the number of peaks. In other words, the crossover time delayed as the total time for runoff event decreased according to the runoff events and dam flush inputs.

The power spectral results assist author's conclusions, and the measurement at a high-frequency (cut-off frequency of ~0.3 hr^{-1}) demonstrates that the streamflow changes at time scales of a few tens of minutes to days. Importantly, the crossover time detected by the power spectral density is comparable with the crossover time detected by the DFA method.

 This study work emphasized the performance of FATS as a robust and effective method for continuous streamflow measurements at a high frequency scale.

CHAPTER 3: Novel high-frequency acoustic monitoring of streamflow-turbidity dynamics in a gravel-bed river during artificial dam flush

3.1 Introduction and purpose

Studying the temporal variability in the dynamics of suspended sediment (SS) is vital to further our information about catchment processes and so understand them comprehensively. Features of a watershed such as its geology, drainage, slope, and land use are all parameters governing the amount and form of sediment transported into rivers [2–4]. Thus, there is a challenge to locate the sources of sediment and where in a watershed erosion and sediment storage are happening. Similarly, calculation and determination of the contribution of streambank erosion to a basin budget is necessary in controlling soil erosion and in introducing suitable mitigation practices to decrease stream SS and associated pollutant load [5,6] and thus improving downstream surface water quality.

Sediment transport during a dam flush (DF) event or due to scouring may have adverse effects on the ecosystem in the downstream river reaches [35]. Bilotta and Brazier (2008) specified that the effects of SS on fish depend on numerous key factors such as the SS concentration and the duration of exposure to it, and the chemical composition and particle-size distribution of the SS. An understanding of the sublethal effects of augmented sedimentation and turbidity dynamics is crucial to enhance our knowledge of the potential impacts of increased sediment loading on stream fish production and how these effects vary among species living in sympatry [37].

During a single hydrological event, analyzing the relationship between suspended sediment concentration (SSC) and discharge (Q) hysteresis is a good approach to understand the properties of sediment dynamics and get information about the underlying geomorphic processes taking place at the watershed scale [38–40]. The suspended sediment concentration and discharge (SSC–Q) hysteresis behaviors (either clockwise or counterclockwise loops) have been attributed to varied phenomena according to the properties of the

watershed area [41,42]. The complex behavior of SSC–Q hysteresis patterns is assessed based on diverse hysteresis-index approaches [42–44]. However, interpreting SSC–Q hysteresis events remains problematic, and hence extra investigations are required to extend our knowledge about the hidden ecological features that are exposed to SS transport.

Turbidity is viewed as a proxy for determining the SS content in rivers by establishing site-specific empirical relationships between turbidity and in-situ measured sediment concentration [45]. Moreover, turbidity observation is widely used to investigate sediment-related hydrological issues. Turbidity estimates can be viewed as an alternative to estimating sediment concentration using direct sampling and subsequent laboratory analysis: in-situ turbidity monitoring methods tend to be low-priced and simpler [46–49]. Moreover, many studies have monitored the dynamics and characteristics of turbidity–discharge (T–Q) and turbidity–rainfall have found very close relationships between turbidity and SSC [48,50–54].

Truthful estimation of the direct and continuous discharge passing through a river cross-section remains a central problem in the field of water-resources engineering. At present, the approach used most to estimate river discharge is the classical rating curve (RC) method. Uncertainty estimation in the RC approach have been studied by [9,55,56]. However, to the best of our knowledge, there is currently no accepted approach to estimating discharge uncertainties. An empirical one-to-one relationship between water level and discharge estimated from rating curves (RC) that is determined under the important assumption that streamflow is steady, therefore, this method may be not precise in the case of streams that are subjected to unsteady flows.

The development of numerous techniques and instruments has led to improved streamflow measurements; Kawanisi et al. [9] have recently demonstrated that the streamflow measured by the FATS changes at very short time scales (i.e. daily and sub-daily scales). In other words, they demonstrated the presence of discharge fluctuations detected by FATS rather than RC discharges that took place over very short time periods. This feature motivated us to observe the variations of streamflow behavior over high-frequency scales (i.e., short time periods of several hours) especially within artificial DF events, and also the scattered

turbidity (T) and discharge (Q) (T–Q) hysteretic behavior related to lag time between peaks of discharge and turbidity.

Therefore, the main aims of this work are (i) to shed light on the characteristics of T–Q dynamics resulting from artificially operated DF events in a mountain river, and (ii) to investigate what information can be realized and observed from streamflow records obtained by FATS compared with discharges measured by means of classic approaches such as the RC method.

3.2 Study site, methodology, and data description

The observations presented herein were performed in the Gono River at the location designated in (Fig. 1.1) and described in (section 3.1 of Chapter 1) using several methods and techniques, thus the author summarized them in the Table.3.1 below. Nonetheless, the author's main interest in this work is to investigate river dynamics within artificial DF events; in particular, to investigate the characteristics of streamflow using a novel acoustic system and the corresponding turbidity dynamics resulting from the DF.

3.2.1   Annual artificial dam-flush events

The Haizuka dam, which is located around 26 km upstream from the study area (Fig.1.1(a)), was flushed once a year individually in 2007, 2010, and 2011. In contrast, the Haji dam (Fig.1.1(a)), which is located around 40.2 km upstream from the monitoring site, was operated once a year in 2008, and 2009, 2012, and 2014 in completely concurrent coupling with the operation of the Haizuka dam, however since 2015, it has been operated in non-concurrent coupling with the Haizuka dam. The discharge patterns from the Haji and Haizuka dams within the studied events are depicted in Fig. 3.1.

3.2.2   FATS measurement campaigns

Field observations by means of FATS were accomplished for the fiscal years of 2011, 2012, 2015, 2016, and 2017. The flow rate was measured continuously, with a time resolution of 10 min for the observed data. To measure water levels at the experiment location, the Acculevels were installed near the two transducers.

The total error band is ±0.1% of the measurement range. Because the full scale was 10 m, the total error of the water level was ±0.01 m water.

3.2.3 Ozekiyama Gauging station records, turbidity and Suspended sediment measurement campaigns

As a reference for the discharge obtained by FATS, the author used the available hourly discharge and hourly turbidity data of the Ozekiyama gauging station (Fig. 1.1(b)) operated by the MLIT. The Ozekiyama discharge records comprise events from 2007 to 2012 and from 2015 to 2017. However, the available turbidity data observed at the Ozekiyama station include only events from 2007 to 2011. It should be mentioned that the river discharge observed at the Ozekiyama station was estimated indirectly based on river-stage measurements through well-established RC equations determined by MLIT, furthermore, the turbidity was measured in FTU.

The turbidity records for the rest of the other observed DF events of 2012, 2015, 2016, and 2017 were carried out by a sonde device (OBS INFINITY-Turbi; JFE Advantech Co, Ltd.). The turbidity sonde is a torpedo-shaped device with multiple probes designed to measure water temperature, depth, and turbidity in FTU. The device has an optical sensor emits light and measures water turbidity as the amount of light back scattering caused by all suspended particles. Data accuracy of the optical sensor is enabled by self-cleans integrated wipers that remove biofouling. The sensor usually installed just one day before each DF event mounted on a durable frame fixed placed in the center of the river cross-section and at 0.2 m above the river bed preventing the device from being shaken (see Fig. 1.1(b)). The sonde was set-up for unattended sampling at 10-min intervals on its internal data logger. Additionally, to verify that within sampling location the lateral diffusion was sufficient to ensure homogenous lateral mixing of suspended sediment, a Rinko profiler (conductivity-temperature-density-turbidity) developed by JFE Advantech Co, Ltd., was used to check turbidity profiles in 10-cm depth-triggered mode. Observation fulfilled through DF events of 2014 every 30 minutes and in 2015 every 15 minutes using four points that are located 200 m apart at the Iwai

bridge revealed in (Fig.1.1(b)). This is very important to identify the stratification of SS particles during flush event.

To determine SSC, water samples were collected manually by means of 1000 mL plastic sampling bottles during dam flush events. In this work, during each DF event data were collected near to the T1 position at the location designated in (Fig.1.1(b)) for the fiscal years of 2012, 2014, and 2015 water samples were taken every 30 min to examine grain size distributions of suspended sediment and SSC. A depth-integrated sampling approach was not needed as suspended sediment was well-mixed during DF events. The grain size of the water samples was analyzed by the laser diffraction and scattering system (SALD-2000J, SHIMAZU Ltd).

Table 1.1 Summary of the observed dam flush (DF) events and the source of collected data during each event.

Flush event	Discharge data reference (Q)		Turbidity data reference (T)		SSC Sampling	ADCP
2007	RC-Ozekiyama	-	FTU-Ozekiyama	-	-	-
2008	RC-Ozekiyama	-	FTU-Ozekiyama	-	-	-
2009	RC-Ozekiyama	-	FTU-Ozekiyama	-	-	-
2010	RC-Ozekiyama	-	FTU-Ozekiyama	-	-	-
2011	RC-Ozekiyama	FAT	FTU-Ozekiyama	-	-	-
2012	RC-Ozekiyama	FAT	-	OBS	Done	-
2014	-	-	-	Rinko profiler	Done	-
2015	RC-Ozekiyama	FAT	-	OBS& Rinko profiler	Done	Done
2016	RC-Ozekiyama	FAT	-	OBS	-	-
2017	RC-Ozekiyama	FAT	-	OBS	-	-

3.2.4 ADCP measurement campaign

In 2015, a commercial current profiler (AquaDopp ADCP; Nortek) was used to measure velocity profiles accurately. The up-looking ADCP was mounted on a durable frame and was installed on the river bed to prevent the device from being shaken, and data were collected at a sampling rate of 14 Hz and in a cell size of 10 cm. The average length and intervals of profile were set to 300 s. The ADCP was located 0.2 m above the bed. The purpose of ADCP measurement is to compare the performance of the FATS velocity records.
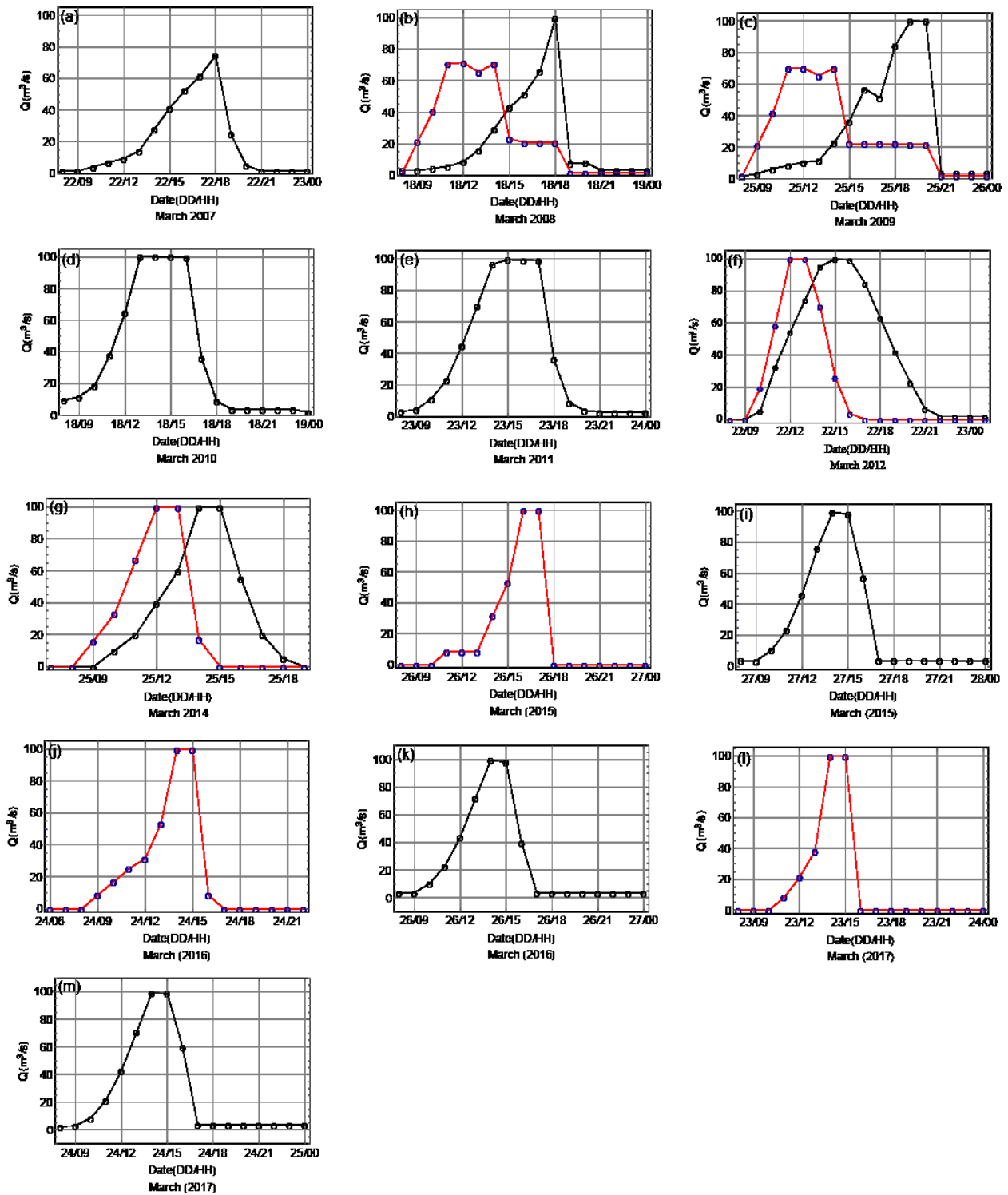
Figure 3.1 Patterns of water discharge from Haizuka (black lines) and Haji (yellow lines) dams during the studied events.

3.3 Results

3.3.1 Streamflow dynamics during dam flush

Figure 3.1 shows the discharge patterns implemented from the point sources (Haji and Haizuka dams). The flush patterns varied throughout the years of the study period, the MLIT purpose to implementing various patterns was to monitor their implications on the growth of new sphagnum. It should be noted that the release of water from the Haizuka dam from 2007 until 2012 was scheduled for 12 h during each event, but that since 2015 the flushing period has been reduced to 6 h. In contrast, the Haji dam was always planned to discharge water for 6 h.

Table 3.2 conveys information about the maximum turbidity values and the maximum discharges observed for each event by both streamflow estimation approaches (i.e., RC and FATS), as well as the lag time between the peak of discharge and corresponding turbidity peaks. Besides, Fig. 3.2 shows the streamflow hydrographs and the resultant turbidity dynamics caused by each event measured at the observation site. In 2007, 2010, and 2011 only one discharge peak can be detected, and the events persisted for 12 h. However, the maximum discharge in 2007 was lower than those recorded in 2010 and 2011 because the maximum flow rate of the released water at that year was 60 m^3/s as opposed to 100 m^3/s in 2010 and 2011. The events of 2008 and 2009 are characterized by a composite flush event because water was discharged from both dams (Fig. 3.1(b) and 3.1(c)) and observed as one peak at the primary monitoring site (Fig. 3.2(b) and 3.2(c)), however water was released from the Haji dam for 6 h, whereas it was 12 h for the Haizuka dam. Alternatively, DF operation in 2012 (Fig. 3.1(f)) was also considered as a composite flush event, nonetheless, two peaks were slightly overlapped and can be clearly observed in the monitoring site (Fig. 3.2(f)).

Table 3.2 Maximum observed discharges of Haji and Haizuka dams by FATS and RC, corresponding maximum detected turbidity for each event, and time difference between discharge and turbidity peaks.

	Flush Event	T_{Max} (FTU)	$Q_{RC\,Max}$ (m^3/s)	$Q_{FAT\,Max}$ (m^3/s)	$\Delta t = t_{Qmax} - t_{Tmax}$ (min)	Notes
2007	Haji Dam	-	-	-	-	-
	Haizuka Dam	25.3	80.52	-	0	-
2008	Haji Dam	92.4	175.3	-	~ 120	Composite Flush
	Haizuka Dam					
2009	Haji Dam	63.3	158.08	-	-60	Composite Flush
	Haizuka Dam					
2010	Haji Dam	-	-	-	-	-
	Haizuka Dam	55.6	176.94		90	-
2011	Haji Dam	-	-	-	-	-
	Haizuka Dam	64.5	166	171	0	-
2012	Haji Dam	54.55	137.18	137.38	~ -90	Composite Flush
	Haizuka Dam	66.68	172.53	188.11	~ -90	
2015	Haji Dam	44.7	122.13	119.55	~ -50	15% of acoustic signals by the FAT were rejected.
	Haizuka Dam	35.82	143.8	146.1	-30	
2016	Haji Dam	39.18	127.25	128.32	-50	-
	Haizuka Dam	28.46	142.55	132.6	-30	-
2017	Haji Dam	28.77	114.5	120.62	-60	-
	Haizuka Dam	30.41	134.6	138.4	-25	-

Since 2011, DF monitoring has been carried out by means of FATS and the RC method. Table 3.2 provides information about the difference between the maximum discharge values detected by the two methods. Interestingly, the streamflow monitored by FATS (Fig. 3.2) exhibited some striking features such as discharge bursts. the author termed these phenomena "discharge shoulders" (DSs) and "secondary discharge peaks" (SDPs) according to the engendered shape, SDPs are thus lower than the primary peaks. In the case of the Haizuka DF events, in 2012, water flushed from the Haizuka dam showed double peaks at the observation location. After the discharge reached its flow peak, it dropped slightly for a short period and then continued almost constantly for roughly 30 min before it peaked again. The observed time

difference between the two peaks was 1–1.5 h, as shown in (Fig. 3.2(f)). This phenomenon was also observed in 2016 from the same dam (i.e., Haizuka). However, the difference then between the two peaks was around 1 h, as shown in (Fig. 3.2(j)). Additionally, the formation of some DSs on short time scales can be seen within the same event (Fig. 3.2(j)). In 2011, the detected SDP was not observed in a similar pattern as in 2012 or 2016. Nevertheless, by visual inspection (Fig. 3.2(e)), two peaks roughly 1.5 h apart can be distinguished, as can be seen the unsteady behavior of the discharge during the flush event within the rising and falling limbs. In contrast, the events of 2015 and 2017 showed no distinctive features. With respect to DF events from the Haji dam, the 2016 hydrograph showed one peak followed by a fall. Nevertheless, within the falling limb, the discharge became roughly constant and persisted for a significant duration of roughly 2 h before it dropped again, forming the obvious DS in (Fig. 3.2(i)). In contrast, this phenomenon is not easily observed in 2015 and 2017. However, in 2012, the falling limb corresponding to the Haji dam overlapped with the rising limb of the flushed water observed from the Haizuka dam.
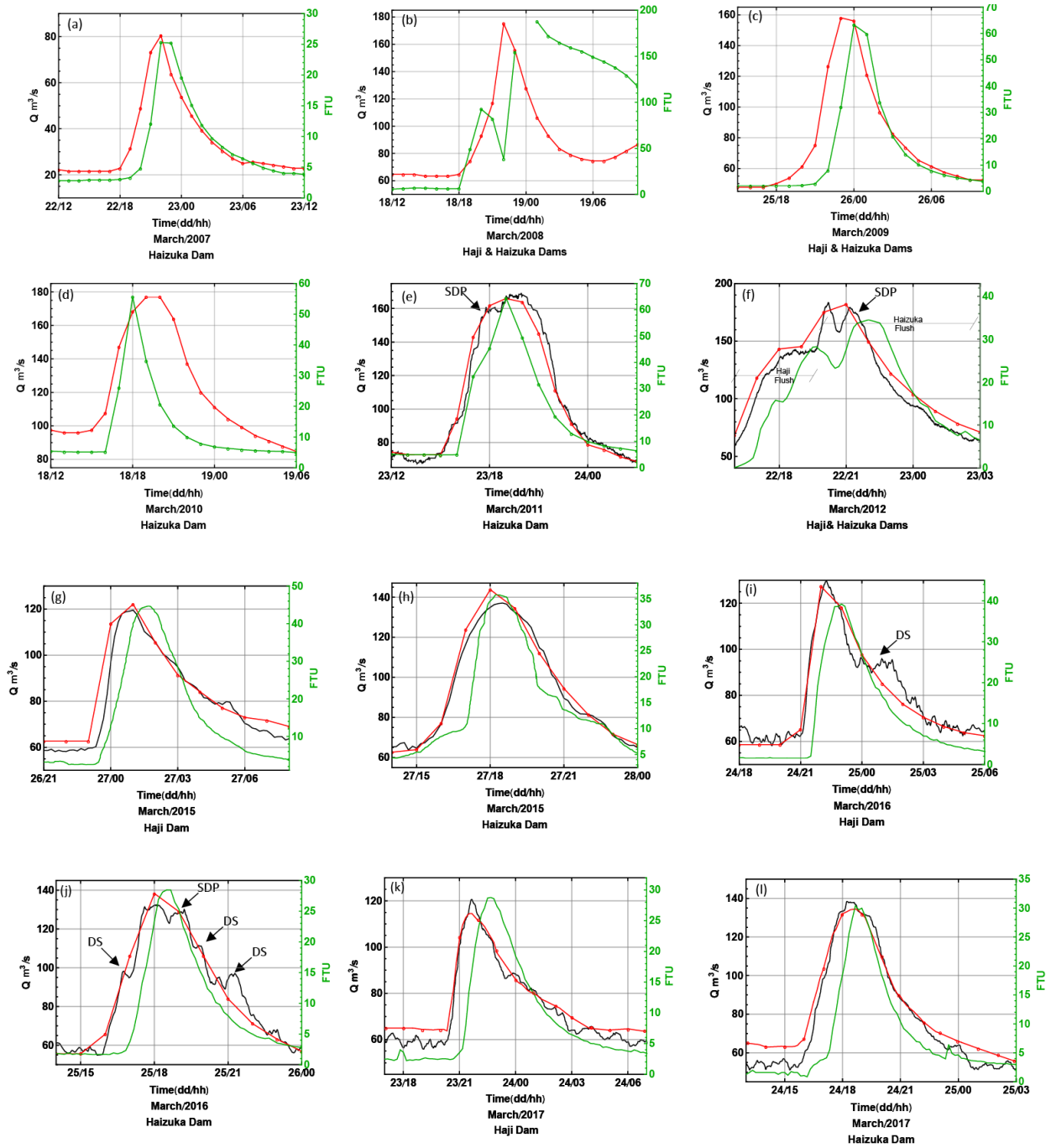
Figure 3.2 Streamflow and turbidity during DF events as measured by FATS (black), RC (red), and turbidity (green). DS = discharge shoulder; SDP = secondary discharge peak. Dots indicate to the hourly data obtained from Ozekiyama gauging station.
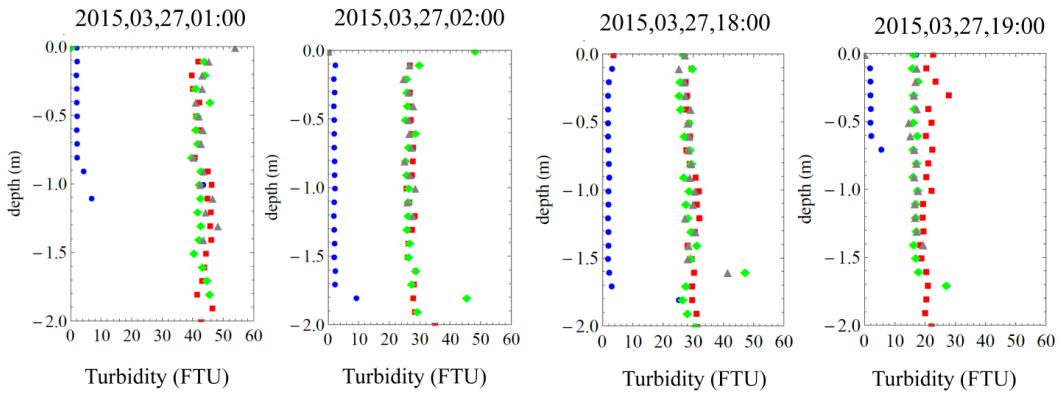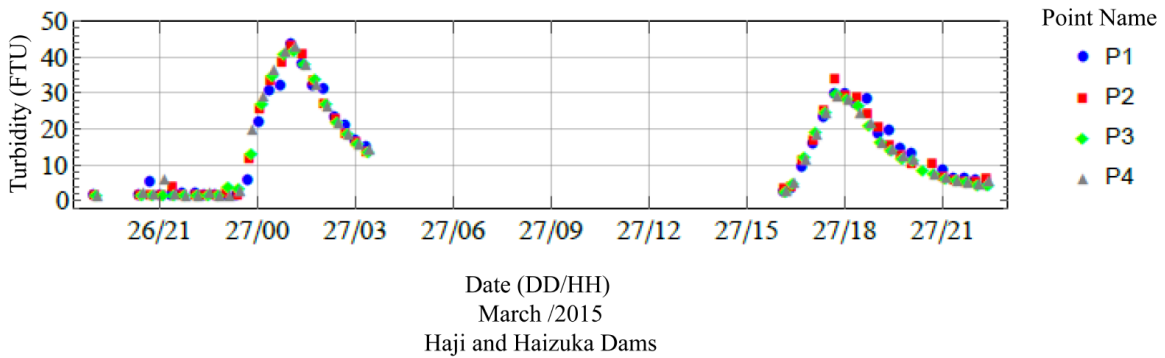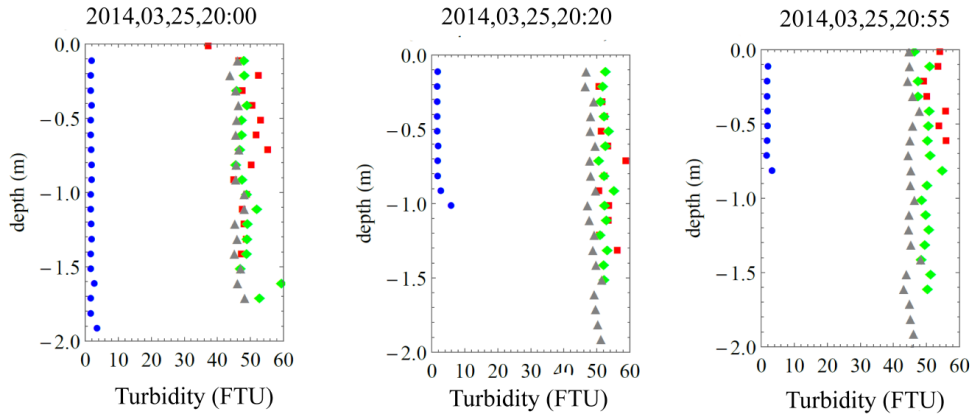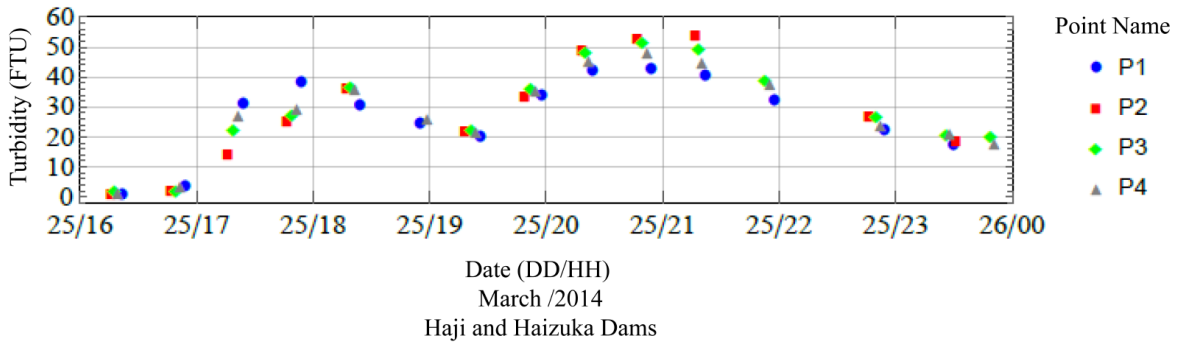
Figure 3.3 Temporal variations in turbidity during DF events of 2014 & 2015 and the vertical profiles of mean streamwise turbidity performed at Iwai Bridge.

3.3.2 Turbidity behavior and turbidity relationship with suspended sediment concentration

During 2014 and 2015 DF events the author observed the turbidity profiles from the Iwai Bridge (Fig.1.1(b)). Figure 3.3 shows the depth-turbidity variations for the studied events (i.e. 2014 & 2015). It can be seen that the turbidity over the vertical and transvers direction are almost same except for the point (P1) which its measurements seems not informative because the readings disproportionate to turbidity estimates obtained by other points (i.e. P2, P3, P4), i.e., the P1 location represents a stagnant water zone or inappropriate observing point which was selected improperly. Fig. 3.3, shows that the turbidity along river cross-section show almost the same vertical and horizontal distribution, that is to say, there is a homogenous mixing of turbidity (and similarly suspended sediment particles). As a result, it can be considered that measuring using a turbidity meter is sufficient and informative to monitor turbidity dynamics. by mounting a turbidity meter on a durable frame fixed and placed in the center of the river cross-section.

On the other hand, the grain size of the water samples during DF were analyzed by the laser diffraction and scattering system, the result of the analysis indicated that the grain size distribution is almost constant with average radius of 19 μm, thus the observed suspended sediment load observed during DF events can be classified as wash-load (wash-load are typically less than 62 μm in diameter). This fact is very important because wash load is carried within the water column as part of the flow, and hence moves with the same average flow velocity of mainstream. Because there is little or no interaction with the river-bed.

Alternatively, regression analysis was performed to observe whether a clear relationship exists or not between streamflow SSC estimates in mg/L, determined from the laboratory analysis, and their corresponding in-situ obtained turbidity measurements collected by the turbidity-meter during the studied DF events. Figure 3.4 shows the comparison between the SSC and turbidity estimates. The determination coefficient is significantly high $R^2 \approx 0.97$. This very good fit reveals that considering turbidity estimates as a proxy for SSC monitoring during DF events is reliable. Interestingly, the regression equation corresponding to the DF event implemented in 2012 disagrees with the regression equation corresponding

to the DF events implemented either in 2014, or 2015. In other words, in 2012 the SSC was about 2.3 times

equals to turbidity concentration, while in 2014, and 2015 DF events the SSC concentrations were

approximately 1.8 times equals to turbidity concentration as indicated by the regression equations as can

be seen in (Fig.3.4).

3.3.3 Turbidity–discharge loops

The maximum values of observed turbidity concentrations during the events of the study are presented in

Table 3.2, and the dynamic behavior within each event is shown in Fig. 3.2. In fact, the recorded turbidity

results give valuable information. For example, in 2007, the maximum recorded turbidity was 25.3 FTU,

which represents the minimum peak among the years of this study. Actually, this value is expected because

the maximum discharged water from the point source (i.e., the Haizuka dam) was 75 m^3/s, which resulted

in a lower turbidity value. Conversely, the maximum observed turbidity peak among the study period was

92.4 FTU in 2008 (see Table 3.2). The flush events from 2015 to 2017 show that the maximum turbidities

declined approximately 50% compared with the events from 2009 to 2012, when the flushing duration was

decreased from 12 h to 6 h.
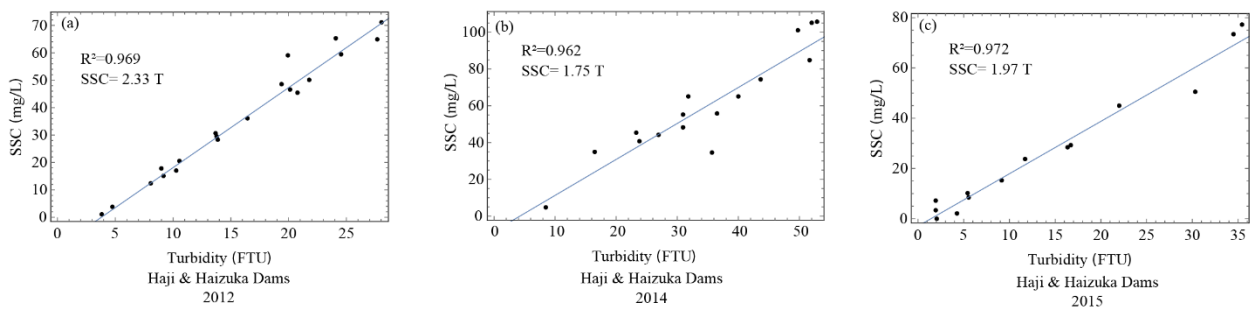
Figure 3.4 Associations between turbidity and suspended sediment concentrations SSC during dam flush events: a) 2012 DF event, b) 2015 DF even, and c) 2015 DF event.

The duration of turbidity change due to flushing is typically a few hours. During that time, the discharge

increases and decreases rapidly, and the lag times between the maximum river discharge and the maximum

turbidity vary by approximately ±1.5 h. Hence, the relationship between turbidity and discharge has the

form of the hysteresis loop presented in (Fig. 3.5). Because the maximum released water from the dam site was 100 m³/s (i.e. artificial and controlled release done according to MLIT's plan), the author normalized the T–Q loops to simplify the assessment of several annual events using the Eq. (3.1) and Eq. (3.2) blow.

$$Q_n(i) = \frac{(Q_i - Q_{min})}{(Q_{max} - Q_{min})} \tag{3.1}$$

$$T_n(i) = \frac{(T_i - T_{min})}{(T_{max} - T_{min})} \tag{3.2}$$

where Q_{max} and T_{max} refer to the maximum discharge and maximum turbidity during a particular event, likewise, Q_{min} and T_{min} refer to the minimum discharge and minimum turbidity during a particular event, while $Q_n(i)$ and $T_n(i)$ are the normalized discharge and turbidity at time i, respectively.

It is important to point out here that because of the overlapping turbidity concentrations induced by DFs and rainstorm in 2008, the corresponding hysteresis loop could not be identified. The disparity in flush patterns seen in (Fig. 3.1) resulted in the various hysteresis loops shown in (Fig. 3.5). Analysis and interpretation of the T–Q hysteresis loops is very important because doing so provides information that helps identify the source of those turbidities during the flush process and that reflects the river-channel scouring and deposition process that occurs within several DF events [40,52,57].
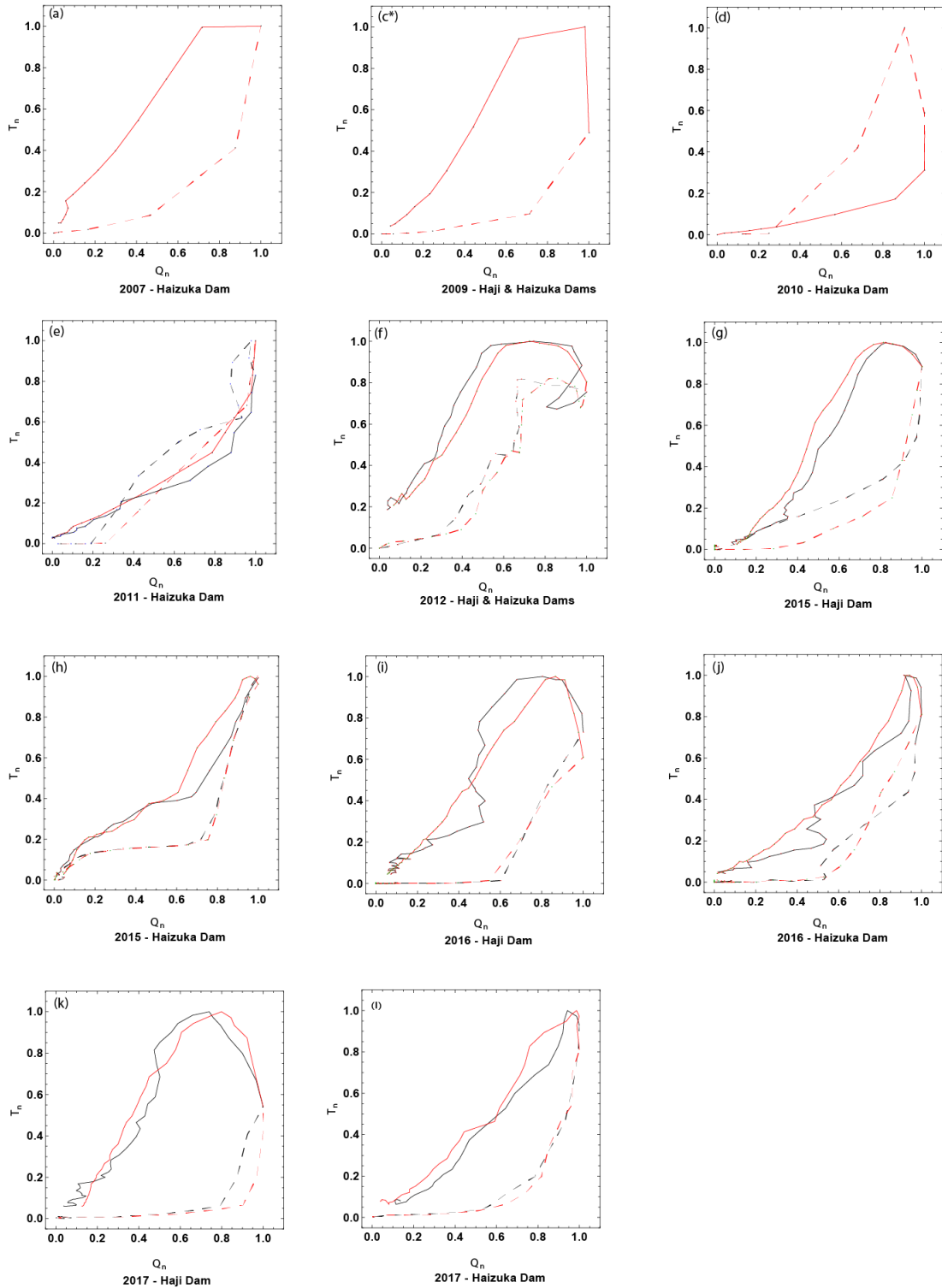
Figure 3.5. Corresponding normalized turbidity–discharge (T–Q) hysteresis during the studied DF events. Red lines are discharges estimated by the RC approach; black lines are discharges estimated by FAT. Dashed lines represent rising limb; continuous lines represent falling limbs. *Because of the overlapping turbidity concentrations induced by DFs and rainstorm in 2008, the corresponding hysteresis loop could not be determined.

55

3.4 Discussion

3.4.1 Evaluation of the FATS performance

As a part of this study is to highlight the performance of the novel acoustic tomography system in continuously monitoring river discharge characteristics, in particular during artificial DF events. Both Table3.2 and Fig.3.2 showed some variations for streamflow hydrographs evaluated by different discharge approaches. The question is whether the findings obtained by FATS are reliable. Indeed, one might doubt the reliability and accuracy of discharge estimates obtained by FATS. However, Kawanisi et al. [7,8] showed FATS to be a powerful tool for monitoring streamflow compared with other discharge measuring approaches. Moreover, Kawanisi et al. [9] discussed fully the error structure in streamflow estimates evaluated by FATS compared with the RC method, namely the errors induced by the section-average velocity component u_m, the angle θ between the FATS transmission line and the stream axis, the mean water elevation h_m, and the mean bed level z_{Bm} along the transmission line. They proved that the largest probable error under low-flow conditions may be estimated as 15%, and thus the main barrier to estimating the uncertainty of a river streamflow measurement in real-life is that the "exact" discharge value is not known. Another important point to note is that while the RC approach assumes that the river flow is steady and depends on establishing a relationship between water level and discharge, discharge estimated by FATS mainly decomposes discharge into two ratings, i.e., velocity and cross-sectional area according to the general discharge equation. Fig. 3.6, shows the relative differences between FAT and ADCP velocity measurements during DF events in 2015. It is very important to remined that during 2015 around 15% of the acoustic data obtained by the FAT system were rejected owing to some technical setbacks. As presented in (Fig. 8 (b)) the relative differences between the VFAT and VADCP are almost within ±10%. As a result, it is believed that FAT is a powerful technique that can be used not only to measure river discharge but also as a promising key technology for investigating various hydrological issues in the field of water resources (Al Sawaf et al., 2017; Bahreinimotlagh et al., 2016; Razaz et al., 2015).
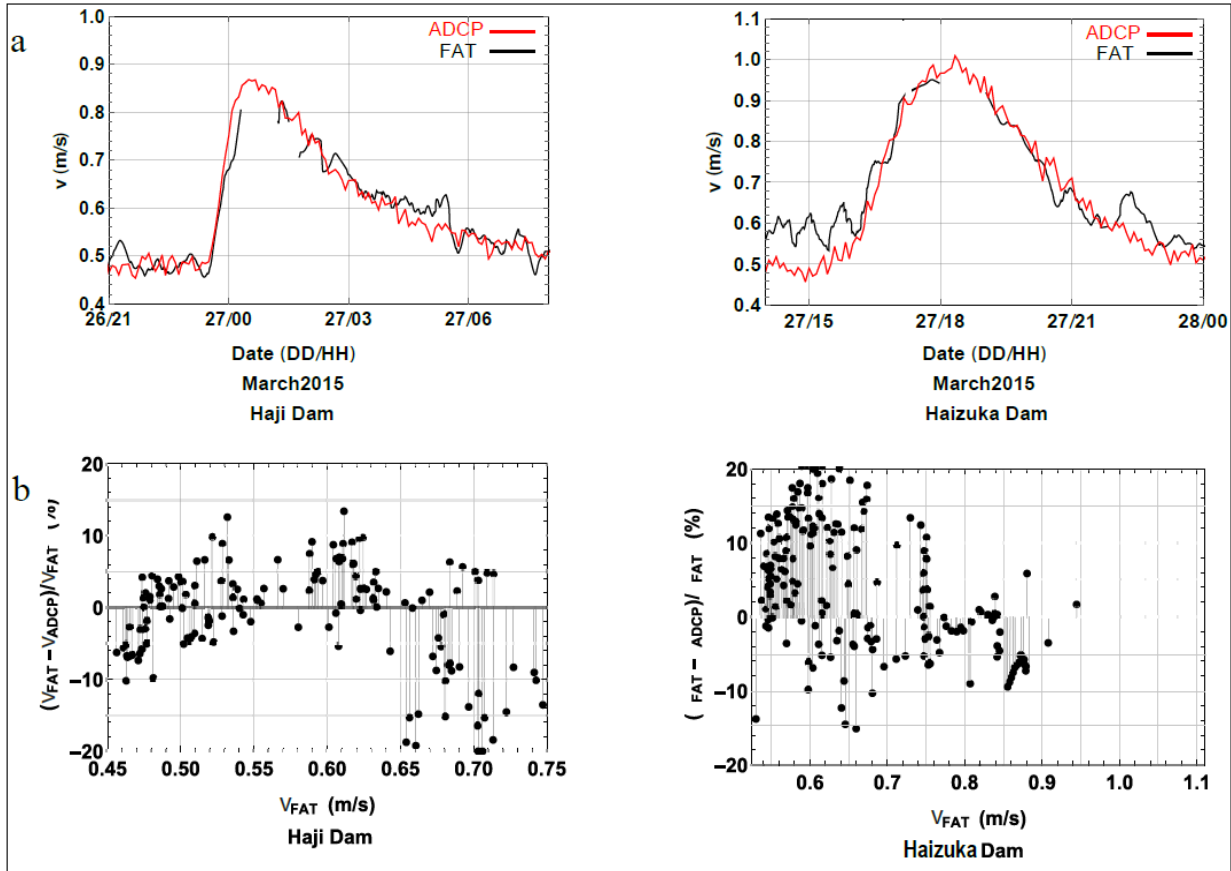
Figure 3.6. Temporal variations in FAT (black) and ADCP (red) velocities, (b) Relative differences between FAT and ADCP velocity measurements.

Al Sawaf et al. [58] have recently investigated the temporal scaling characteristics of river discharge evaluated by both FATS and RC in the Gono river and found that the streamflow measured by FATS showed distinct temporal scaling on short time scales up to roughly 10 h compared with the corresponding discharge time series estimated by the RC method. Therefore, this finding supports the reliability of measurements performed by FATS, especially regarding the presence of short-wavelength irregularities on short time scales in the discharge hydrograph observed by FATS, such as the SDPs and DSs that can be seen in (Fig. 3.2). Therefore, another question that arises is what induces the SDPs and DSs? Currently, in the author's opinion, this might be justified by the flow resistance which determines the amount of water that a river channel can convey through its influence on stream velocity and so flow depth (Powell, 2014). The resistance impact on discharge parameters is usually described by resistance coefficients such as

Manning n. Some works have been revealed that the resistance coefficients have been shown to vary during flood wave propagation (Fread, 1975). On the other hand, the physical interpretation of Manning coefficient is still not perfectly understood.

Worldwide, several scholars have proposed different approaches with the aim of avoiding the direct estimation of resistance coefficient that relate discharge or velocity of a stream to its hydraulic geometry according to Eq. (3.3) (López et al., 2007):

$$Q = K.A.R^{\alpha}.S^{\beta} \tag{3.3}$$

where Q is discharge (m³/s), A is the cross-sectional area (m²), R is the hydraulic radius (m), S is the friction slope, and α and β are exponents for the Manning equation, expressed in SI units, α= 2/3, β = 1/2 and K = 1/n, where n is the Manning resistance coefficient.

In general, the devised approaches by previous works can be divided into two main methods. The first method tried to estimate the Manning coefficient by correlating n with some of the independent variables of Eq. (3.3), S and R. Another alternative approach ought to define flow resistance equations without explicit estimation of the resistance coefficient, i.e., to fit the parameters of Eq. (3.3) (or of the equivalent equation that takes the cross-sectional average stream velocity as a dependent variable) explicitly through regression. These methods have been summarized beneficially by López et al., (2007). In the case of our work, we examined the temporal velocity variations during DF events in 2016 for both Haji and Haizuka Dams following the empirical equation developed by (Bray, 1979) using records from numerous gravel-bed rivers in Alberta, Canada presented in Eq. (3.4):

$$V = \frac{1}{n}.d^{0.67}.S_w^{0.32} \tag{3.4}$$

where V is the mean cross-sectional velocity (m/s), d is the mean river depth (m), R is the hydraulic radius (m), S_w is the average longitudinal slope of the water surface for the reach, and $\frac{1}{n}$ = 9.6 estimated using best fitting regression.
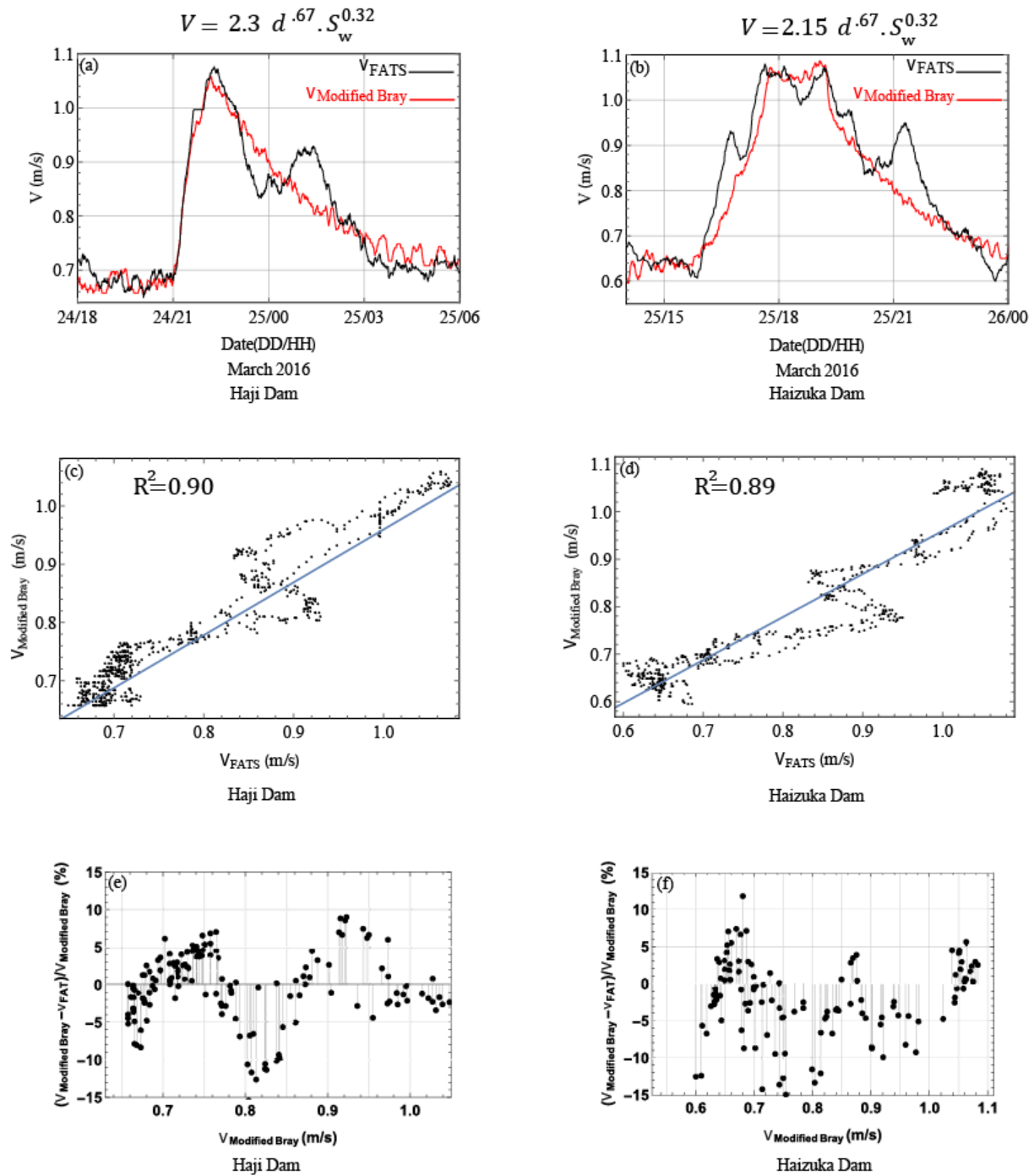
Figure 3.7. Temporal variations in VFAT and VBray(a)-(b), associations between VFAT (m/s) VS VBray (c)-(d),

and (e)-(f) relative differences between VFAT and VBray velocity estimations.

In fact, it can be noticed very high correlation between stream velocity estimated by FAT and their counterpart velocities evaluated by the empirical equation proposed by (Bray, 1979) with determination coefficient which of $R^2 \approx 0.90$ (Figs.3.7 (c), (d))., However, in the case of our stream the Bray's equation was modified empirically through direct regression to improve the velocity estimation in the case of our stream as presented in (Figs. 3.7(a) , (b)). Moreover, Figs. 3.7 (e) and (f) show that the relative differences between the V_{FAT} and V_{Bray} ranged approximately between -15% and 10%. This finding indicates that the trend of n versus flow rate Q may be during falling or rising depending on the geometry of wetted area, and the variation in water level between either bank of the river and also on the river-bed characteristics along the transmission line between the installed acoustic transducers.

The key feature of measuring stream velocity and discharge by means of FAT is more useful because streamflow estimated by FAT mainly decomposes discharge into two ratings, i.e., velocity and cross-sectional area according to the basic discharge equation. Hence, additional considerations for the temporal variations in water slope and variations of Manning roughness over different stages may interpret in detail the reason behind several characteristics and performance of SDPs and DSs. Accordingly, further monitoring for unsteady discharge coupled with continuous stream velocity variations and drops in water level during the course of flood wave propagation is still required in such a relatively small and medium watersheds for short time scales will be deemed in the future observation programs.

3.4.2 Interpretation of turbidity- discharge hysteresis

Dams control a wide range of physicochemical characteristics, especially in its downstream reaches. On the other hand, trapped sediment leads to various unavoidable physical and environmental degradation in the lower stream reaches of the dam area and at the dam itself. Indeed, SSC and water turbidity are critical parameters in regulating ecological systems. However, the purposes of DFs (e.g., crop irrigation, water supply, flood control) have an enormous impact on different characteristics related to sediment dynamics. Typically, dams are flushed to mitigate sediment accumulation in reservoirs. Hence, the amount of released sediment is expected to be very high. However, in the case of the Gono River, artificial DFs are performed

once a year from the Haji and Haizuka dams to enhance the growth of sphagnum on the bedrock in streams, this being a food source for theYamame and Ayu sweetfish.

In fact, the high correlation between SSC and turbidity as demonstrated in (Fig. 3.5) enabled us to assess the catchment erosion and sediment transport dynamics based by studying their T-Q hysteresis patterns. Generally, most of the studied artificial DFs from the Haji and Haizuka dams mainly showed (negative) anticlockwise hysteresis and absence of clear clockwise hysteresis in our monitoring site. However, in 2010 (Fig. 3.2(d)), although turbidity started to increase slightly after the streamflow increment (i.e., the flowrate started to increase at 15:00 while the turbidity started to increase at around 16:00 and peaked at 18:00 before the streamflow reach its maximum at approximately 19:30, the turbidity peak during that event peaked earlier at 18:00 before the discharge reached its maximum peak at approximately 19:30, consequently forming a figure-of-eight loop (Fig. 3.5(d)). In 2011, both discharge and turbidity peaked almost concurrently (Fig. 3.2(e)). Thus, the outputted hysteresis was represented by a very narrow figure-of-eight loop, although the dissimilarity between the estimated Q_{FAT}, and Q_{RC}, hydrographs affected the hysteresis shapes (Fig. 3.5(e)). Interestingly, since 2015 the hysteresis loops associated with the Haizuka dam have taken the form of a narrow crescent, whereas the hysteresis patterns induced by the Haji dam have had wider loops. The reason for this is simply the relatively long distance between the Haji dam and our observation point (~40 km). This means a longer delay time between the discharge and turbidity peak and thus a wider loop, and vice versa in the case of the hysteresis due to the Haizuka dam, which is roughly 25 km from our observation site. The diversiform of the studied T-Q loops obtained either by FATS or RC method give motivation to analyze these disparities by means of hysteresis index [42,63], these loops may reflect important information especially in the presence of DSs or SDPs, however, due to the paucity of discharge data obtained by FATS this will be considered for future works.

Mainly, in the case of our observation site located in the Gono River, DFs result in anticlockwise hysteresis loops at the observation locations shown in (Fig. 1.1). However, only two events exhibited a figure-of-eight pattern. Williams [64] reported that at least one of the following reasons may cause anticlockwise

hysteresis: (i) seasonal distribution of sediment production within the drainage watershed; (ii) different travel times for the flood wave and the sediment flux, particularly in view of the downstream distance between the flood source and the measuring station; (iii) high soil erodibility in combination with protracted scouring during the flood. Meanwhile, other studies have concluded that anticlockwise hysteresis loops relate to (iv) prolonged erosion processes during extended storm events, or (v) sediment being supplied from more-distant sources (associated with extended travel times), channel bed erosion [40,65,66]. Therefore, several reasons for these various forms T-Q loops can be discussed as follows.

Firstly, sediment transport during artificial DF events were not subjected to seasonal effects, thus according to Williams [64] seasonal distribution of sediment production within the drainage watershed does not seem a reason behind anticlockwise T-Q loop. According to MLIT, sediment was not released from dams during any of these studied DF events. As a result, the important point regarding sediment and turbidity dynamics of this study is the location and source of the observed turbidities associated with the discharged water from both dams. Unfortunately, neither sediment nor turbidity monitoring had been performed by the MLIT. Secondly, prolonged erosion processes during extended storm events does not seem to be a reason because dam flush period is short (i.e. less than 12 hours).

The author measured turbidity concentrations associated with the Haizuka dam in 2017 near the Minamihatashiki gauging station (Fig. 1.1(a)). As can be seen in (Fig. 3.8). the turbidity at this site measured by (RBR *solo* TU) in NTU. Unfortunately, the accumulation of vegetation debris on the sensor made some technical setbacks, thus the recorded turbidity estimates after 17:50 were rejected. Also, there was no calibration between the measurements in FTU obtained from our primary observation location and turbidity estimates in NTU obtained from this site.

It can be seen in (Fig. 3.8) that the turbidity peak was observed at the Minamihatashiki gauging station at 16:50 while discharge peak corresponded to water release from the Haizuka DF peaked at 17:40, thus there is a 50-min difference before the discharge reached its maximum level. This clockwise hysteresis may attribute to a rapid response system (short distances between sediment source and receptor) thus the peak

of turbidity precedes the maximum streamflow of the event. Fast response systems are characterized by fast sediment flushing and depletion in the river network because of a limited supply of readily available material for transport [40,65,67]. Alternatively, this peak observed at our primary site on (24 March 18:58) i.e. 128 min lag between the maximum turbidity at Minamihatashiki station and turbidity peak at our location. Given that the waterway distance from Minamihatashiki station to our observation site (Fig. 1.1(b)) is around 6.85 km and the average velocity measured by FAT during the DF event was approximately 0.88 m/s, the required time for turbidity peak to be observed from Minamihatashiki station at our observation site is 130 min. Accordingly, sediment being supplied from more-distant sources may represent a reason for counterclockwise hysteresis at least during 2017 because wash load is carried within the water column as part of the flow, and thus moves with the average velocity of mainstream. Because there is little or no interaction with the bed, the particles extract only negligible momentum from the flow.

As a result, in the case of our monitoring point (i.e. near Ozekiyama st.), since the author recognized several hysteresis loops (i.e. counterclockwise and complex hysteresis loops) with different lag times, it can be thought that anticlockwise hysteresis in our case are likely generated by sediment being supplied from more distant sources located in some places after the dams and alongside the river pathway in several sites upstream to our observation site, as well as by channel bed erosion as described by [40,64,65]. Also, the events of 2008, 2010, and 2011 had short time differences between the arrival of the turbidity and discharge peaks. Therefore, the author conclude that the sediment in these studied DF events was generated mainly throughout the river channel during DF, i.e., high soil erodibility. Nevertheless, additional sediment monitoring alongside the river channel would be required to gain better insights into the interactions between discharge properties and the linked sediment behavior within each event.
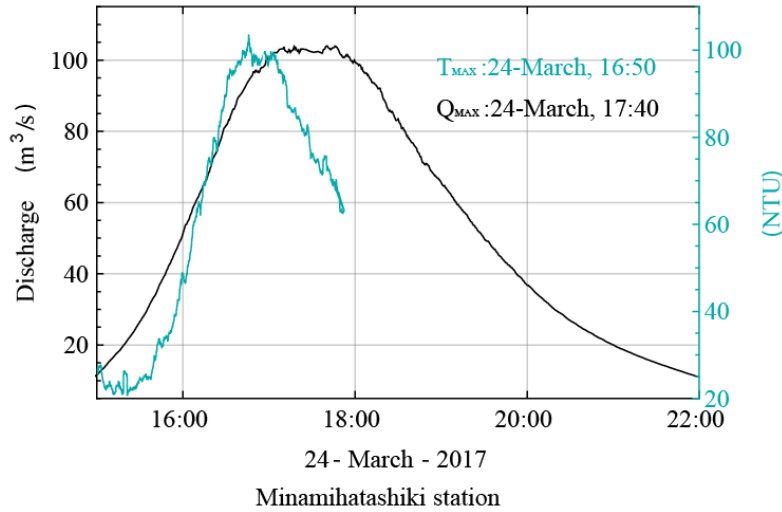
Figure 3.8 Temporal variations in water discharge and turbidity at Minamihatashiki station.

3.5 Conclusions

Understanding the properties of turbidity–discharge (T–Q) dynamics associated with dam flush (DF) entails long-term information and continuous monitoring of the underlying turbidity and discharge processes. The present work presents and discusses the authors' field investigations toward understanding streamflow and turbidity dynamics in a gravel-bed river during artificial DF operation by using a sophisticated discharge measurement system. Several lessons were learned from this filed monitoring project are summarized below.

This work highlights the potential advantages of streamflow monitoring by means of a new competitive technology namely the Fluvial Acoustic Tomography (FAT) system in the Gono River which is a shallow gravel-bed river in real time at high-temporal resolution. In general, cross-sectional average velocity estimated from FAT data were in high agreement with the velocity observed by ADCP system since the relative differences between the V_{FAT} and V_{ADCP} are almost within ±10%. As a result, it is believed that FAT is a powerful technique that can be used to measure river discharge accurately.

The observed flush patterns of discharged water showed considerable variation between flushing point and the observation station. Interestingly, new phenomena were documented in this study that were not detected by the rating curve (RC) approach, namely the presence of discharge secondary peaks (SDPs) and discharge shoulders (DSs) within DF events for streamflow measured by means of the FAT. These features are induced by the flow resistance which determines the amount of water that a river channel can convey through its influence on stream velocity and hence streamflow within a DF event. Based on our findings, the cross-sectional velocity of stream estimated by FAT provides tolerable when compared to Bray's velocity formula that defines flow resistance in gravel bed-rivers. This finding is very important because it indicates that the trend of n versus flow rate Q may be during falling or rising depending on the geometry of wetted area, and the variation in water level between either bank of the river and also the river-bed characteristics along the transmission line between the installed acoustic transducers. Moreover, it was found that the developed Bray's formula in estimating average cross-sectional velocity in gravel-bed rivers was beneficial with improving the 1/n coefficient from best fit regression.

Despite their limits, suspended sediment concentrations during DF events were measured mainly by means of turbidity as a proxy proved to be reliable. On the other hand, the diversiform of T–Q hysteresis loops reflect the variations in channel scouring and deposition within flushing periods. According to the sequence of peak turbidity and discharge, mainly anticlockwise T-Q relationship hysteresis were observed, which was the most common type. Sediment during the studied DF events was generated mainly throughout different locations of the river channel from river banks because only wash load were observed. Finally, our findings may open up a new possibility of dynamically monitoring unsteady flows during the course of flood wave propagation for lower watershed scales in the world.

CHAPTER 4: Monitoring of streamflow-stage hysteresis behavior of a gravel-bed river

4.1 Introduction and purpose

Rating Curves method (RC) is one of the most common classical methods used to provide continuous measurement of river discharge based on one dimensional view (1-D) of a river. The basic assumption method presumes that river is flowing under steady and uniform conditions. However, the steady and uniform behavior of flow assumption of RC approach is not valid in natural streams in most cases. The cross-section and water slope are changeable in longitudinal direction and hence the discharge varies in time. According to the simple continuity equation of discharge, if a given discharge has to pass through less cross-sectional area, the reduction in area must be offset in part by an increase in velocity in order to balance the discharge, velocity and channel area relationships. Conversely, a variety of parameters that are independent of channel cross section, such as slope or roughness, can lead directly to changes in the velocity of a flow. The advanced streamflow instrumentations (e.g. acoustic velocity meters (AVMs), acoustic doppler current profilers (ADCP), etc.) gives rise to improve the quality of estimated measurements allowing to application of the Index Velocity Rating Curve method. Estimating streamflow using Index Velocity Rating Curve differs from the conventional RC method by separating velocity and area at a specific cross-section into two ratings-the index-to-mean velocity rating and the stage-to-area rating [68]. Hence, the multiplication of these ratings, i.e. river average velocity V and the cross-sectional area A, gives the temporal variations in discharge Q at that location.

A conventional slope area method has been basically used to estimate streamflow peaks based on high-water marks after large flood events. Thus, this approach estimates a peak discharge according to Manning equation based on the measured specific in-situ river channel characteristics of the cross-section, channel roughness, and the friction slope. Notably, the application of conventional slope area method assumes that channel non-uniformity is properly accounted during the computation of the friction slope [69].

Recently, the Continuous Slope Area method (CSA), has received increased interest with presence of the low-cost pressure transducers that directly measures water surface slopes [61]. For example, Smith et al.[61] measured the streamflow variations by means of CSA approach deploying 8 pressure transducers at both sides of river banks at 4 subsequent cross-sections on the Babocomari River (Arizona, USA) in 2002. They demonstrated that CSA method can be utilized to estimate a continuous discharge hydrograph and to generate a steady RC. Just recently, Lee et al. [60] monitored the un-steady behavior of streamflow using 2 pressure transducers positioned at both river banks on the Clear Creek near Oxford (Iowa, USA) by implementing the CSA method. They concluded that CSA approach might be a promising method for dynamically tracking unsteady water surface slopes and flows in natural streams, however, they reported that additional studies are still needed to increase the accuracy of the CSA method in future research.

Therefore, the main purpose of this work is to monitor the unsteady behavior of streamflow, as well as, hysteresis in streamflow-stage in such a relatively small mountainous watershed using discharge data obtained from two methods: (i) CSA method generated from RC discharge data, and (ii) Index Velocity Rating Curve discharge data obtained by means of a novel acoustic tomography system (FATS), for different scales of rainfall events.

4.2 Study region, methodology and measurement description

The observations presented herein were performed in the Gono River at the location designated in (Fig. 1.1) and described in (section 3.1 of Chapter 1). Since our primary goal in this study is to monitor the discharge-stage hysteresis behavior, the author will utilize two methods to estimate discharge: (i) The proposed CSA method suggested by Lee et al. [60] and (ii) discharges estimated by our acoustic tomography system based on the Index Velocity Rating Curves.

4.2.1   Principle of the CSA method

This method utilizes the Manning's equation given in Eq. (4.1) as:

$$Q = \frac{1}{n} A R^{2/3} S^{1/2} \tag{4.1}$$

where Q is the discharge passing through a specific cross-section, n is the Manning's roughness coefficient, A is the cross-sectional area, R is the hydraulic radius and S is the friction slope.

The friction slope presented in Eq. (4.1) is equivalent to the water surface slope or the streambed slope. Nevertheless, natural channels in observation areas are often nonuniform, thus the consideration of this method is valid if energy loses from the energy gradient are considered in the estimation of the friction slope as given in Eq. (4.2):

$$S = \frac{h_f}{L} = \frac{\Delta h + \Delta h_v - k(h_v)}{L} \tag{4.2}$$

where h_f is energy loss due to boundary friction in the reach, Δh_v is the difference in velocity head at the two sections, $k(\Delta h_v)$ is the energy loss due to shrinking or expansion of the reach ($k = 0$ for contracting reaches and $k = 0.5$ for expanding reaches), and L is the length of the reach.

Channel nonuniformity effects can be reduced by evaluating the geometric mean of the channel conveyance, at the two cross-sections. Hence, the discharge can be calculated as shown in Eq. (4.3) as:

$$Q = \sqrt{K_1 K_2 S} \tag{4.3}$$

where K_1 and K_2 are the channel conveyance at the two cross-sections.

4.2.2 The proposed CSA approach by Lee et al [60]

Fig. 4.1 presents step-by-step the implementation procedure of the proposed CSA method by Lee et al [60], this approach can be summarized according to the following steps: the first step comprises selection of a suitable monitoring site. Dalrymple and Benson[69] as well as ISO 1070 [70] determined site selection criteria that satisfy the conventional slope-area method. The next step then is deployment of water level loggers (pressure transducers). In fact, installation of a set of at least 3 pressure transducers to measure stage and water surface slope (upstream, downstream, and in the middle of the selected reach) is recommended, thus increasing the number of the installed pressure transducers is important to address any peculiarities in estimating discharges and to improve reliability in the case of instrument failures [61,71].
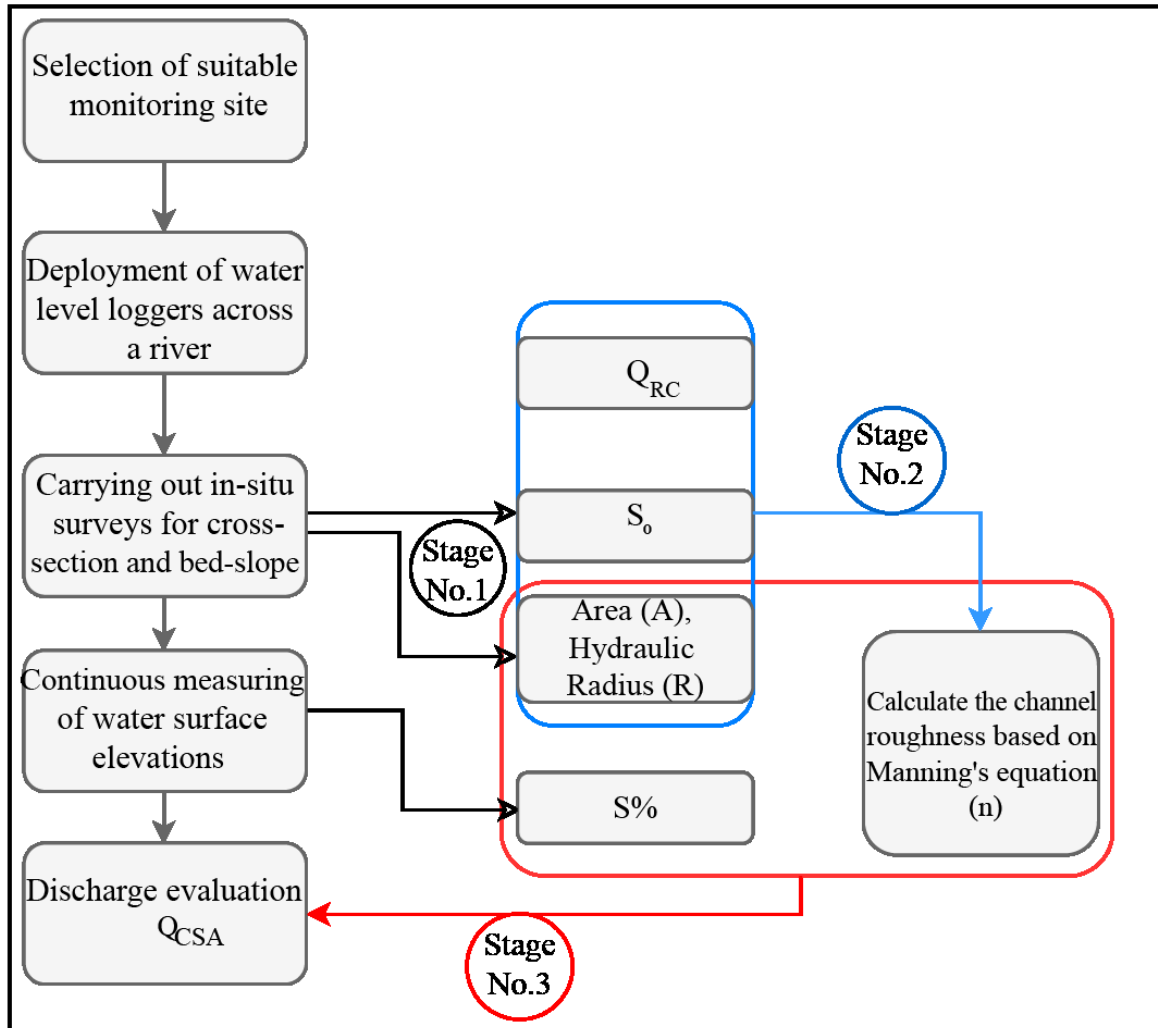
Figure 4.1 A schematic diagram illustrates step by step implementation of the proposed CSA method.

In the case of our observations water-level data were collected every 30s using submersible level transmitters (Acculevel ACL-10- A; Keller America, Inc.). The acculevels were installed diagonally across the river banks with a horizontal distance of 294.56 m between of them. The total error band was ±0.1% FS. Because the full scale was 10 m, the total error of the water level was ±0.01 m. It is presumed that using two sensors provide the needed indication of the hysteretic behavior [60].

Once water loggers deployed, the third step is to perform a geodetic survey to record the water surface elevation at each logger tip. It is necessary in this step also to carry out a channel bed slope S_0 survey for discharge estimation. The next step is to perform continuous cross-sectional area A and hydraulic radius R

measurements be-tween water level sensors. The available measured discharge data from a nearly gauging station (Ozekiyama gauging station) were used to deter-mine the channel roughness based on Manning's equation Eq. (4.1). The surveyed channel bed slope, area, and hydraulic radius are used as in-puts for these calculations. Performing this step (i.e. stage No.2 indicated in Fig. 4.1) will result in a relationship between stages and channel rough-ness coefficients. In the last step (Stage No.3), the unsteady behavior can be estimated at each time step by substituting the constant bed slope with the dynamic water surface slopes and applying the same measured area, hydraulic radius, and estimated channel roughness coefficients. The properties of channel non-uniformity can be minimized by calculating the geometric mean of the channel conveyance based according to Eq. (4.3).

4.3 Results and discussion

Fig. 4.2 (a,b,c) reveals streamflow hydrograph estimates of 3 different scales of different rainfall events evaluated by three discharge methods namely, RC, CSA, and FATS. While it is not our goal in this study to investigate about the accuracy of each discharge method, it is important to point out that Kawanisi et al. [72] fully discussed the error structure in streamflow estimates evaluated by FATS compared with the RC for one month. those errors induced by the mean water elevation h_m, the area A_B of the river bed along the transmission line, the section-average velocity component um, and the angle θ between the FATS transmission line and the stream axis. It was reported that the largest possible error may be evaluated as 15% even in low-flow condition, thus discharge obtained by FATS is reliable. Moreover, it was demonstrated that the relative difference between Q_{FATS} and Q_{RC} does not exceed 6% for Q_{FATS} averaged for 20 h. Also, in Fig. 4.2 (a, b, c) it can be clearly noticed that discharge estimates by RC and FATS show very good agreements for the studied events. This is can be justified mostly by the ideal location of Ozekiyama gauging station for discharge measurement selected by MLIT to establish discharge rating curve equations.
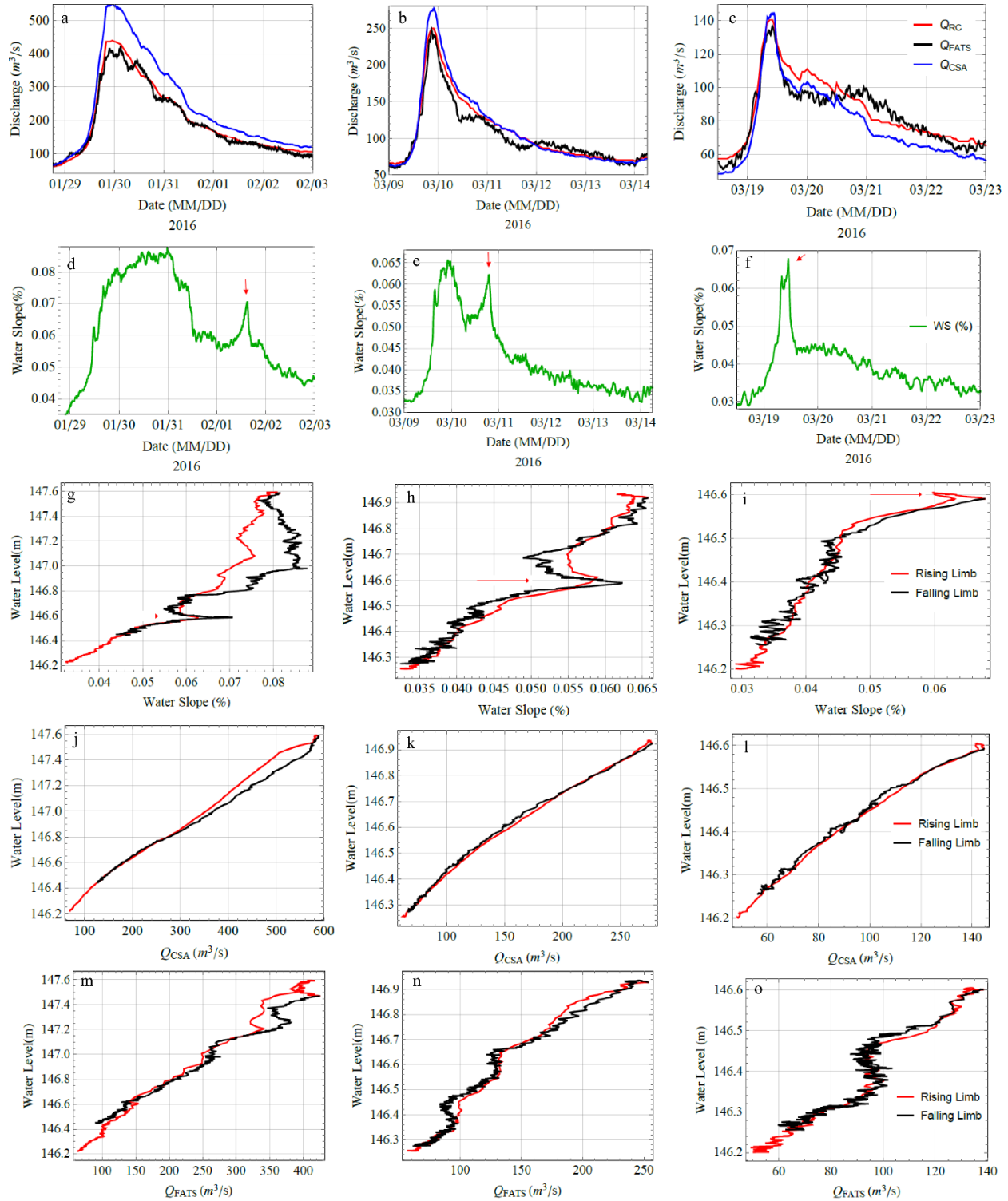
Figure 4.2 Discharge hydrograph for the studied events, corresponding water slope patterns, water slope-stage hysteresis, QCSA-stage hysteresis, and QFATS-stage hysteresis.

Discharge estimates obtained by the CSA approach were in good agreement with Q_{FATS} and Q_{RC} except for the large flood event as shown in the first case. This is may be justified since CSA method assumes discharge passing through a cross-section of a river channel is steady and uniform, nonetheless, given the fact that natural streams are invariably non-uniform. The temporal variations in water slope for the studied events graphs Fig. 4.2 (d,e,f), exhibit striking features. Within each single rainfall event it was observed two peaks. The first peak shows the temporal variations in water slope that are linked to the discharge peak, however, the water slope varied according to the intensity of each event. The second peak indicated by red arrows that can be detected in the falling limb. It can be observed that the second peaks are not coincide or subjected to the maximum streamflow peak. Additionally, these secondary peaks are characterized by sharp vertex vary for a few hours (sub-daily variation). Of interest, the behavior of this secondary peak can be realized obviously in the water slope-water level hysteresis graphs Fig. 4.2 (g, h, i). In other words, these secondary peaks always show a roughly constant increasing behavior at a fix water-level (WL=146.6 m). This phenomenon may be induced by the conditions where the water level in the channel is controlled by local objects such as rapid, bed friction and/or channel shape, thus inducing sudden decreases in slope due to channel contraction or expansion.

Although the hysteresis patterns are nested within rising and falling limb revealing complex loop, a positive behavior can be observed for all studied events. Besides, it is observed that the water slope-stage hysteresis loop increases as the scale of rainfall event becomes greater.

Streamflow-stage hysteresis comparison for discharges estimated by both CSA and FATS during the study events are provided in (Fig. 4.2 (j,k,l)) and (Fig. 4.2 (m,n,o)) respectively. In the case of discharges evaluated by CSA approach it can be seen that discharge-stage loops are very narrow except for the large-scale rainfall event. In addition, a quasi-steady state relationship between streamflow and water level can be observed. This may be justified due to the CSA approach itself. In other words, discharge estimated by CSA method in this study were indirectly computed based on discharge data obtained by Ozekiyama gauging station which evaluated according to Rating Curve approach, i.e. establishing a relationship

between river stage and discharge. As a result, the unsteady behavior detected here is basically affected by the temporal variation in the channel's water surface slope determined according to the CSA method. On the other hand, streamflow-stage hysteresis patterns estimated by means of FATS exhibited completely unsteady behavior, this finding seems to be confirmed with Al sawaf et al· [58] who studied the temporal scaling characteristics of river discharge observed by both FATS and RC in the Gono river, and found that the streamflow measured by FATS showed distinct temporal scaling on short time scales up to roughly 10 h compared with the corresponding discharge time series estimated by the RC method. Similarly, Kawanisi et al[7] reported that the streamflow measured by FATS changes at time scales of a few tens of minutes to days. Furthermore, it can be clearly confirmed that streamflow-stage loops estimated by FATS increases as rainfall event scale increases. However, during the low scale rainfall events, the hysteresis loop is not informative, i.e. the direction of hysteresis loop cannot be detected. Nonetheless, a clockwise hysteresis loops can be observed within the mid and large-scale events.

4.4 Conclusions

In this study, the author provide a contribution toward monitoring the unsteady behavior of discharge-stage hysteresis in a relatively small mountainous river. In order to monitor the unsteady behavior of streamflow, two methods were used: (i) the (CSA) method, and (ii) Curve discharge data obtained by means of a novel fluvial acoustic tomography system (FATS).

Major conclusions can be summarized as follows:

1. Temporal variations in water slope graphs during a single hydrological event exhibit two peaks. The first peak is subjected to the observed streamflow peak. Whereas, the second peak where observed in the falling limb and likely to be induced by the backwater effects.

2. Water slope-stage hysteresis patterns showed that the first water slope peak conveys information

about the water slope-water level dynamics with "positive" or clockwise behavior, i.e. water level maxima precedes water slope peak. Meanwhile the second peak showed increasing of water slope over a certain water level.

3. Streamflow-stage hysteresis for discharges estimated by CSA method had very narrow loops increases with large-scale rainfall events. Additionally, a quasi-steady state relationship between streamflow and water level can be observed.

4. Streamflow-stage hysteresis for discharges estimated by means of FATS approach exhibited unsteady behavior. Similarly, the hysteresis loop increases with large-scale rainfall events.

5. Finally, it was demonstrated that FATS has high performance in detecting the unsteady behavior of streamflow than CSA method.

CHAPTER 5: Monitoring stage-discharge hysteresis versus stage-water surface slope hysteresis during single hydrologic events in a gravel-bed river

5.1 Introduction and purpose

To assess the dynamics of rivers, an accurate characterization of river discharge during unsteady flow regimes is of paramount importance. Therefore, comprehensive knowledge of streamflow and its associated uncertainties are crucial for water resources engineering applications. In fact, the common classical approach that is widely practiced to providing continuous measurement of river discharge is the Rating Curve (RC) approach [73]. The RCs are constructed through periodic direct streamflow measurements carried out at convenient times, under the assumption that river flows under steady and uniform conditions. Alternatively, the stage-discharge RC should be frequently re-determined with new parameters for the changed topography and stream characteristics. Consequently, maintaining the accuracy of discharge estimated by means of the RC is labor intensive and time-consuming [18].

It has been reported that there are glitches associated with RC approach, particularly for unsteady flows such as those occurring during floods [74]. For example, during flood events (rainfall, dam flush, etc.), unknown uncertainties in RCs method ensue from several reasons: (i) natural uncertainties induced by randomness of natural processes (turbulent fluctuation, wind effect, geometrical shape of the river cross-section, etc.), (ii) insufficient knowledge of the physical processes of the river system, (iii) measurement uncertainties: due to inaccurate measurement of water level or flow, inaccurate spatial or temporal sampling for stream parameters (water level, stream velocity, etc.) [75], and importantly (iv) the fact that most of the calibration measurements for RCs are achieved during quasi-steady flow situations happening in normal flows, however during high floods, in most cases the establishment of the RCs are accomplished based on a limited sample of direct measurements [74], which imply error during these intense events.

Once a flood wave passes through a stream, the wave front approaching a cross-section will have an increase in velocity as discharge reaches to its peak, the rear of the water discharge reduces its velocity. This

acceleration-deceleration sequence of the flow generates a loop in the stage-discharge relationship [62]. This loop is the representation of the unsteady flow behavior produced during flood wave propagation [74].

In fact, limited works had documented the presence of streamflow-stage hysteresis that have been mostly acquired in few sites over the world, especially where located on large rivers aimed to provide more precise measurement for streamflow forecasting models. Nevertheless, the unsteady behavior of streamflow-stage hysteresis has received low concern in medium and small-scale watersheds. Moreover, it was found in chapter 4 that streamflow-stage hysteresis loops estimated by FATS are informative more than streamflow-stages estimated by the CSA method.

This point inspired the author to extent my investigation program and write this chapter which is a complementary chapter for the previous chapter (i.e. chapter 4). This chapter presents and discusses the author's field investigation program during which a FATS was deployed to monitor and observe the streamflow-stage hysteresis in a mountainous shallow river, and the corresponding water slope-stage hysteresis loops as well. The hysteresis loops during flood events will be useful for interpreting the spatial distribution of streamflow fluctuations during high-frequency scales. The novelty of the present study lies in the successful application of a tomographic instrument in an extremely shallow river to report the unsteady behavior of streamflow in such a moderate mountainous watershed during different scales of rainfall events and to report the connection between of the streamflow-water level (Q-WL) loops with surface slope-water level (WS-WL) dynamics for a full fiscal year of different seasons. Therefore, the objectives of this chapter are to: (1) identify and classify the major types of single-event (Q-WL) and (WS-WL) relations, using models and field examples; (2) provide a simple graphical explanation for each type; and (3) summarize physiographic or hydrological reasons for each type. The single hydrologic event is considered in this chapter a flood lasting days.

5.2 Study region, data description, and methodology

5.2.1   Study area and data description

The observations presented herein were performed in the Gono River at the location designated in (Fig. 1.1) and described in (section 3.1 of Chapter 1). In this chapter, discharge measurements by FATS comprises the records of the fiscal year of 2016, with a time resolution of 10 min for the observed data. Similarly, at the experiment location, the Acculevels were installed near the two transducers. The total error band is ±0.1% of the measurement range. Because the full scale was 10 m, the total error of the water level was ±0.01 m water. Water level record covers the events of 2016 and the time resolution of 10 min for the observed data.

Water surface slopes between transducers (T1&T2) (Fig.1.1) were computed according to Eq. (5.1) below:

$$WS\% = \frac{WL_1 - WL_2}{L} \tag{5.1}$$

where *WS%* is the water surface slope, WL_1 and WL_2 are the water levels at T1 and T2 respectively, *L* is the horizontal distance between the T1 and T2.

Beside to discharge and water slope measurements, turbidity measurements were carried out during June and July 2016 (Fig1.1) by a sonde device (OBS INFINITY-Turbi; JFE Advantech Co, Ltd.) in FTU. The role of the turbidity measurements is to check whether a direct correlation between water slope variations and the temporal variations of turbidity is existed or not.

5.2.2   Methodology

Although the findings of this chapter will be presented in terms of categorizes of (*Q-WL*) and (*WS-WL*) relations, the approach in reaching at those patterns was a graphical procedure. The first step, temporal variation graphs of *Q* coupled with *WL* and *WS* coupled with *WL* for a single hydrologic event were plotted. Then for the same event, temporal variations of *WL* versus *Q* are plotted with *WL* on the *Y*-axis and *Q* on the *X*-axis. Finally define each type of hysteria and compare of the different generated cases. Only the more common hysteresis patterns will be examined in this work.

5.3 Result and discussion

Lee et al. [60], proposed a new approach to monitor the unsteady flows (i.e., hysteresis) during the course of flood wave propagation.

In this study, for a single rainfall event, water slope dynamics was plotted and compared with the corresponding temporal water level variations, then plot the association between water slope and water level to check if any hysteresis is existed. Similarly, for the same rainfall event, streamflow hydrograph was plotted and compared with the corresponding temporal water level variations, then plot the association between streamflow and water level to check if any hysteresis is existed. The hysteresis refers to a looped stage–discharge rating caused by unsteadiness of flows, the detected hysteresis in their method is directly influenced by the hysteresis behavior of water surface slope-stage estimates.
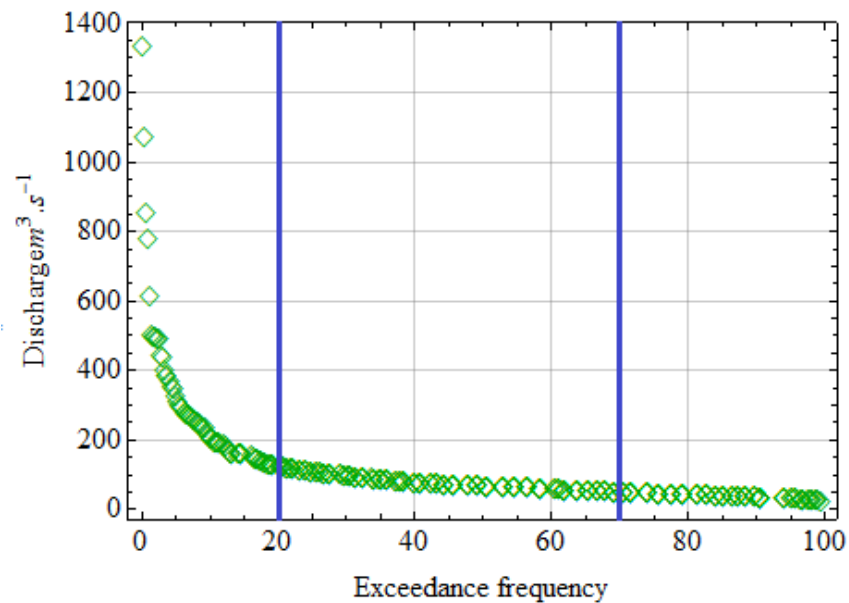
Figure 5.1 Flow Duration Curve for the Fiscal year 2016.

During 2016, 41 single hydrological events was examined. Through this year, river discharge varied according to the different rainfall scales varied from low intensity to very high intensity events. Thus, the flow duration curve (FDC) was used to select the threshold among three different flow types into: (i) low

discharge intensity (Q≤ 49 m^3. s^{-1}), medium discharge intensity (125 <Q> 49 m^3. s^{-1}), and high discharge intensity events (Q> 125 m^3.s^{-1}) as shown in Fig 5.1.

The capability of the watershed to provide flows of various magnitudes and the percentage of time river flow exceeds a specific value was expressed by the FDC. The shape of the FDC curve presented in Fig.5.1 in its upper region shows very step curve, indicating rain-caused floods and intermittent regime [65].

The 41 analyzed events showed different discharge-water level hysteresis loops. The selected events indicate for 4 different hysteretic behavior can be categorized as:

(i) No hysteresis: both streamflow and water level peak together or almost together at same time

(ii) Clockwise hysteresis: If the streamflow monitored by FATS peaks before the water level reach to its peak

(iii) Counterclockwise hysteresis: water level peaks earlier than streamflow, and

(iv) Figure-of-eight or complex loops.

However, in some events discharge by FATS signals was lost. Similarly, the corresponding water slope-water level hysteresis loops showed 4 different hysteretic behavior can be categorized as:

(i) No hysteresis: both water surface slope and water level peak together or almost together

(ii) Clockwise hysteresis: If the water slope peaks before the water level reach to its peak

(iii) Counterclockwise hysteresis: water level peaks earlier than water slope, and

(iv) Figure-of-eight or complex loops.

Table 5.1 conveys information about the studied 41 events for the fiscal year 2016 classified by their occurrence. Also, the table shows information of the maximum discharge by Q_{FATS} and the corresponding water level by observed at the Ozekiyama gauging station, besides, the stage-discharge hysteresis direction as well as the stage-water slope hysteresis direction.

Table 5.1 The studied hydrological events in 2016, and the observed hysteresis during each event; 0; no hysteresis, +: clockwise hysteresis, -: counterclockwise hysteresis, *: complex hysteresis. Blank cells indicate for the loss of FATS signals.

Month	Event No.	Q_{FATS}	WL Ozekiyama	Discharge Hysteresis Type		Water slope Hysteresis Type	
January	E1	105.94	147.19	No Hysteresis	0	No Hysteresis	0
	E2	408.58	148.59	Clockwise	+	Clockwise	+
February	E3	351.9	148.31	No Hysteresis	0	Clockwise	+
	E4	258.04	147.97	Counterclockwise	-	Clockwise	+
March	E5	253.5	147.89	No Hysteresis	0	Complex loop	*
	E6	137.44	147.41	No Hysteresis	0	Clockwise	+
April	E7	65.13	146.87	Complex loop	*	No Hysteresis	0
	E8	60.3	146.84	Complex loop	*	No Hysteresis	0
	E9	187.2	147.69	Complex loop	*	Clockwise	+
	E10	97.58	147.14	Complex loop	*	No Hysteresis	0
	E11	101.73	147.12	Clockwise	+	Clockwise	+
	E12	195.42	147.62	Counterclockwise	-	Clockwise	+
	E13	227.96	147.83	Complex loop	*	Complex loop	*
May	E14	131.2	147.36	Complex loop	*	Complex loop	*
	E15	72.5	147	Complex loop	*	Complex loop	*
	E16	225.37	147.82	Clockwise	+	Counterclockwise	-
	E17	262.35	147.95	Clockwise	+	Clockwise	+
	E18	73.98	146.95	Complex loop	*	Counterclockwise	-
	E19	77.21	147.03	Complex loop	*	No Hysteresis	0
June	E20	108.16	147.2	No Hysteresis	0	No Hysteresis	0
	E21	403.44	148.39	Clockwise	+	Clockwise	+
	E22	183.42	147.64	No Hysteresis	0	Clockwise	+
	E23		149.55			Complex loop	*
	E24	267.12	147.93	Complex loop	*	Complex loop	*
July	E25	458.77	148.78	No Hysteresis	0	Counterclockwise	-
	E26	611.07	149.11			Counterclockwise	-
August	E27		146.82			No Hysteresis	0
	E28		147.14		-	No Hysteresis	0
September	E29	102.74	147.26	Complex loop	*	No Hysteresis	0
	E30	129.06	147.51	Complex loop	*	No Hysteresis	0
	E31		150.75			Complex loop	*
	E32	109.24	147.24	Complex loop	*	No Hysteresis	0
	E33					No Hysteresis	0
October	E34		148.39			Clockwise	+
	E35		148.07			Counterclockwise	-
November	E36	109.88	147.32	No Hysteresis	0	No Hysteresis	0
	E37	65.27	147	No Hysteresis	0	No Hysteresis	0
December	E38	50.1	146.87	No Hysteresis	0	No Hysteresis	0
	E39	111.06	147.29	No Hysteresis	0	No Hysteresis	0
	E40	115.14	147.31	No Hysteresis	0	No Hysteresis	0
	E41	337.8	148.27	Complex loop	*	Complex loop	*

To gain better understanding about the river discharge dynamics, water surface slope hysteresis (*WS-WL*) of the studied events were classified and compared with their corresponding streamflow dynamics (*Q-WL*) as presented in some examples of Fig. (5.2), Fig. (5.3) and Fig. (5.4) below.

5.3.1 No hysteresis

The simplest type of (*WS-WL*) relation is the single-valued line or no hysteresis. This type can be observed when water surface slope and water level peak together or almost together. When (*WS-WL*) has no hysteresis Fig.5.2 (d, e, f), the corresponding (*Q_FATS-WL*) also has no hysteresis pattern as illustrated in Fig.5.2 (j, k, l). Though, it can be realized that during low rainfall intensity of the events (light discharges), do not resulted in any apparent hysteresis form. Therefore, in the case of no hysteresis loops the rainfall event intensity is low.
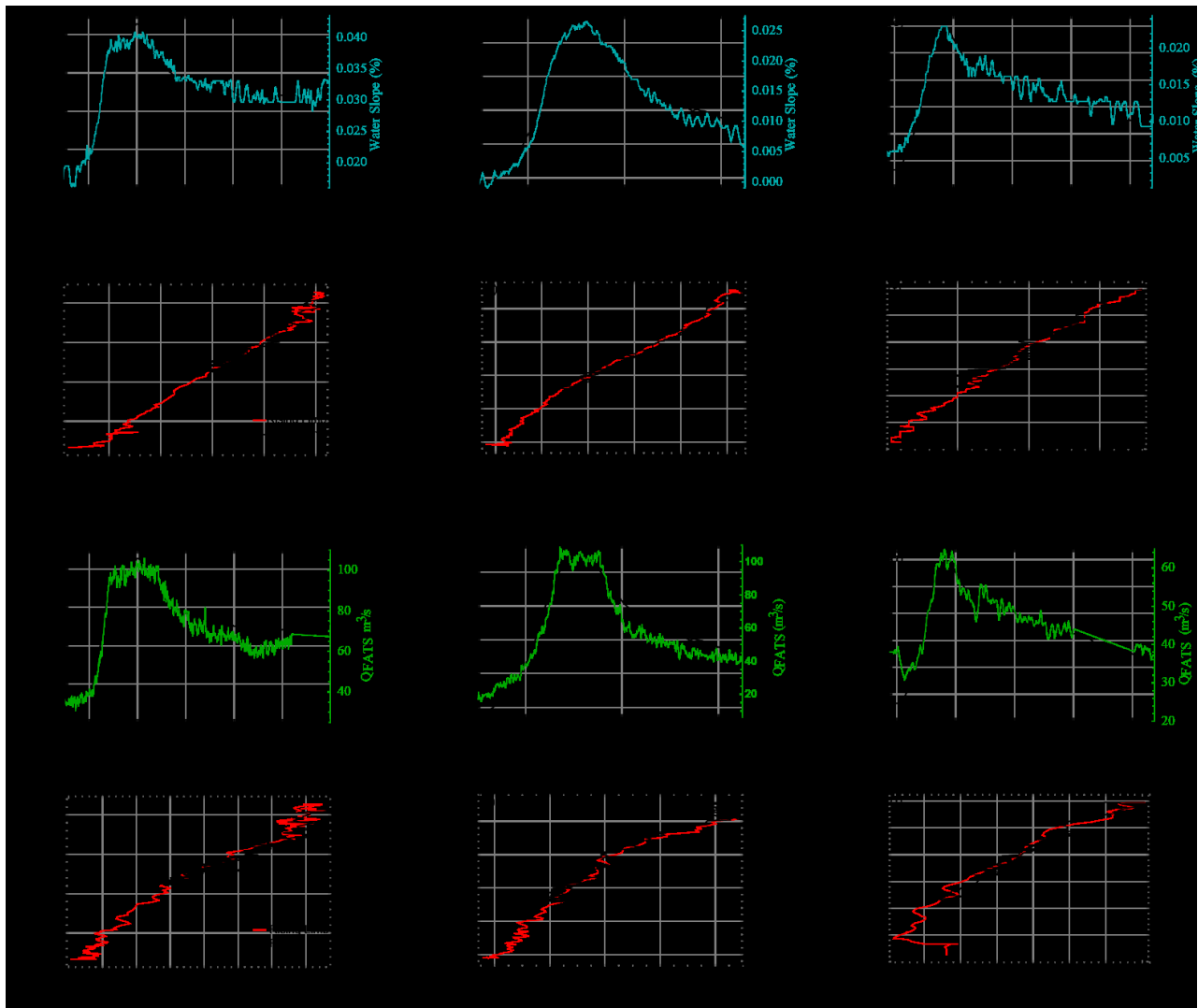
Figure 5.2 Temporal variations in water slope, corresponding (WS-WL) hysteresis, temporal variations in streamflow, and corresponding (QFAT-WL) hysteresis, (Case I: No hysteresis of WS-WL).

5.3.2 Clockwise hysteresis

In this case, water slope peak arrives at the stream cross section before the water level. In this type, when (*WS-WL*) forms clockwise hysteresis Fig.5.3(d, e, f), the corresponding (*Q_FAT-WL*), however, formed either (a) clockwise hysteresis Fig. 5.3(j), or (b) no hysteresis as shown in Fig.5.3(k), or even (c) counterclockwise loop, as can be seen in Fig.5.3(l), hence it seems that there might be no direct relationship between the (*WS-WL*) loops and (*Q_FATS-WL*).
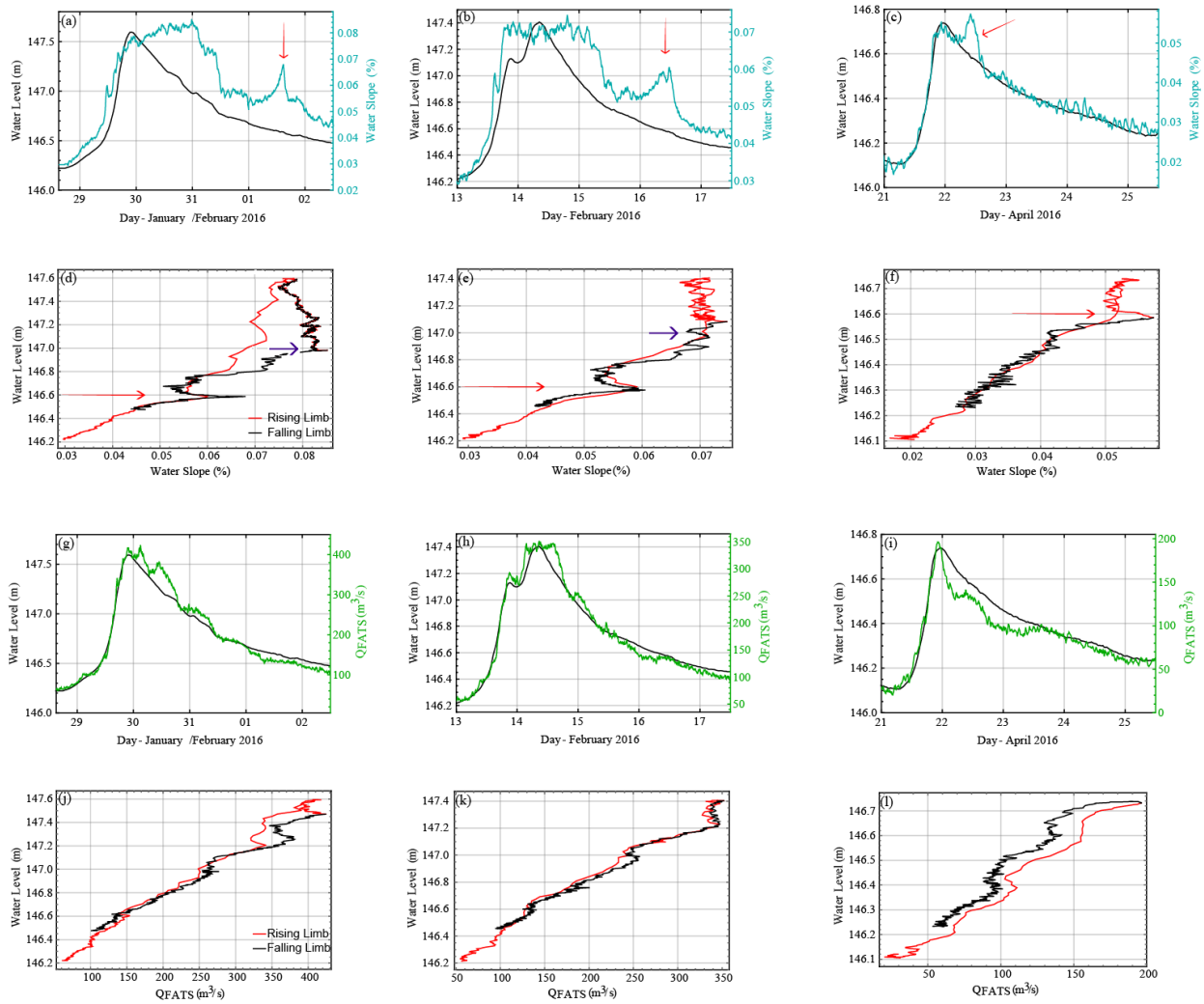
Figure 5.3 Temporal variations in water slope, corresponding (WS-WL) hysteresis, temporal variations in streamflow, and corresponding (QFAT-WL) hysteresis, (Case II: Clockwise hysteresis of WS-WL).

Nevertheless, two distinctive features can be observed during the medium and high intensity rainfall events, the temporal variations in the water slope have two peaks, (i) the first peak corresponded to the maximum peak of runoff induced by the rainstorm event, (ii) the second peak (see Fig.5.3(a, b, c) red arrows) that were realized at a specific level (WL≈ 146.6 m), these secondary peaks are characterized by sharp vertices vary for few hours (sub-daily variation). The secondary peak here increases and decreases significantly whenever water level approaches that level (i.e. $WL \approx 146.6$ m) Fig.5.3(d, e, f), suggesting that this feature is influenced by backwater effects refer to condition where the water level in the channel is not controlled by local objects such as rapids, bed friction or channel shape, but instead by downstream conditions, i.e. backwater effects here caused by sudden decreases in slope, channel contraction or expansion. In addition, another interesting feature can be detected when (WL= 147 m, indicated by purple arrows). That is to say, in the case of high intensity rainstorm events and whenever water level become equal or greater than (WL=147 m), water slope become constant ($WS \approx$ 0.065-0.069%) as water level is greater than that level as shown in Fig.5.3 (d, e).

5.3.3 Counterclockwise hysteresis

In this case, water slope peak arrives at the stream cross section after the water level peak. Alternatively, in the case (WS-WL) forms counterclockwise hysteresis Fig 5.4(d, e, f), the corresponding (Q-WL) formed either (a) clockwise hysteresis Fig. 4(j), or (b) no clear hysteresis were observed as Fig 5.4 (k, l). This result seems to be consistent with the pervious result, that it seems that there is no direct relationship between the (WS-WL) loops and (Q-WL), furthermore, it can be concluded that the patterns of (WS-WL) hysteresis do not necessarily to have same direction of their corresponding (Q-$WL)$ loops. Similarly, for both medium and high intensity flows two peaks were observed exactly similar to (WS-WL) Clockwise hysteresis, however, in the case of (WS-WL) has anticlockwise hysteresis it can be seen clearly that whenever ($WL \geq$ 147 m) the water surface slope become almost constant ($WS \approx$ 0.068 %) as water level increased.
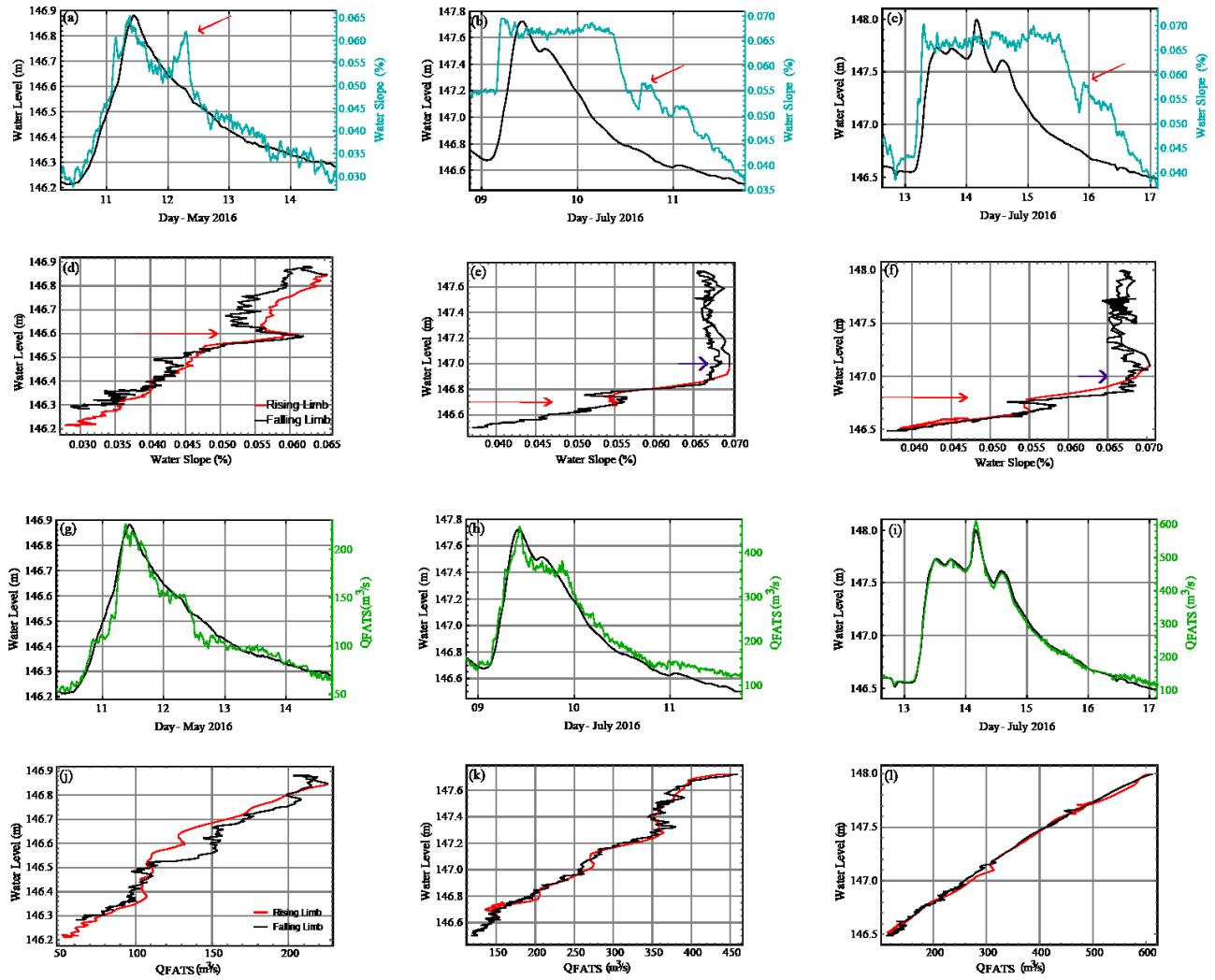
Figure 5.4 Temporal variations in water slope, corresponding (WS-WL) hysteresis, temporal variations in streamflow, and corresponding (Q_{FAT}-WL) hysteresis, (Case III: Counterclockwise hysteresis of WS-WL).

Deciphering meaning of helical loops as identified with acoustical measurement equipment is not popular yet. In fact, the presence of, and reason for the primary and secondary circulation stress vectors has been rarely tackled by a few researchers, and likely has water flow physics to explain these phenomena. Since the time frame during the Ph.D. course was not enough sufficient to investigate more, the author would defer to, and suggest the individuals who are interested in this phenomenon seek those who have, or their papers of documentation to clearly explain these phenomena.

However, the water surface slope staying relatively constant at high stages is probably during periods when the floodplain or relatively flat floodprone area adjacent to, and above the bankfull flow rate, is accessed, so the valley gradient or floodprone surface is a major factor. During less than bankfull flows, the water surface gradient is controlled more by the series of materials controlling riffle tops in the channel. In step - pool morphology, the top of steps are areas of water surface gradient abrupt change. Indeed, it is difficult to measure conditions with abrupt change, but the water surface slope in the extreme channel gradient changes of falls and cascades should show areas with much higher water surface gradients, but how can these be measured? It is important to check Japanese national classification of watershed scales (small, moderate, high, etc.) to map the hydrologic units from region, basins, sub-basins, watersheds and sun-watersheds.

Indeed, our discharge observations performed by FATS system and the observed water slope hydrographs open up a new opportunity of dynamically observing unsteady flows (i.e., Stage-Discharge hysteresis) during the course of flood wave propagation. Hence, additional consideration for of the temporal variations in water slope may interpret the reason behind different performance of unsteady flows. Thus, further monitoring for unsteady discharge coupled with continuous stream velocity variations and drops in water level during the course of flood wave propagation is still required in such a relatively watershed for short time scales.

5.3.4   Comparing water surface slope dynamics to another mountainous river

In order to increase understanding about water surface slope dynamics and its connection to streamflow dynamics, additional observation was carried out at the Basen River. The Basen River which is a tributary for the Gono River, is also a mountainous gravel-bed river. Unlike the Gono River which has a catchment area of 3900 km^2, Basen River has a watershed area of 680 km^2.

The location of experiment is illustrated in Fig 5.5, the Acculevels were installed diagonally (S1-S2). The total error band is ±0.1% of the measurement range. Because the full scale was 10 m, the total error of the

water level was ±0.01 m water. Water level and water slope measurements started from August 1st, 2017 to the end of March 2018, and the time resolution of 10 min for the observed data.
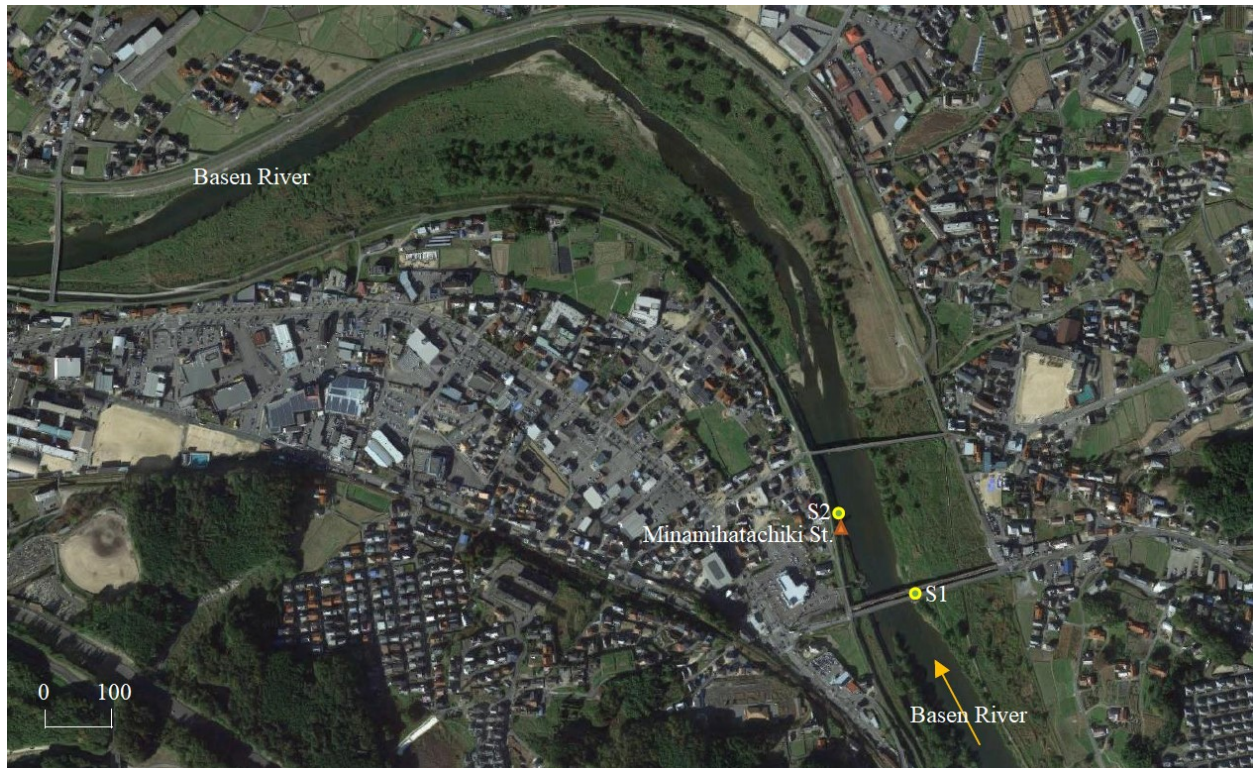
Figure 5.5 The Basen River and places of water level loggers, and the Minamihatachki station

It was noticed that the water surface slope dynamics is considerably affected by the watershed area. For example, Fig. 5.6 shows the time-series of the temporal variations of water levels and water surface slope during different periods recorded in the Basen River. As can be seen in (Fig 5.6 a), apparently the red arrows indicate for 7 different rainfall events, however, the temporal variations in water surface slope obtained for the same period only indicate for one significant event occurred on 18th September 2017, meanwhile other event negligible impact (see Fig.5.6 b). During 18th September, over bank flow occurred, however, as can be seen in Fig. 5.7, the hysteresis behavior for such high intense flood cannot be easily understood or captured though it has counterclockwise direction. Likely in another event happened on 23rd October which characterized by lower intensity than the 18th August event. Therefore, it can be inferred that for small

basins water slope hysteresis cannot be documented easily, the water surface slope dynamics are not informative in small basins and no clear hysteresis loops can be observed.

Similarly, Fig. 5.6 c shows the temporal variations of water level recorded during January and February 2018 for the same river. Obviously, the water levels ranged between 1.3 to 1.65 m. The corresponding temporal variations in water slope can be detected by in very tiny scales (i.e. 5×10^{-3}%) as shown in Fig .5.6 d.
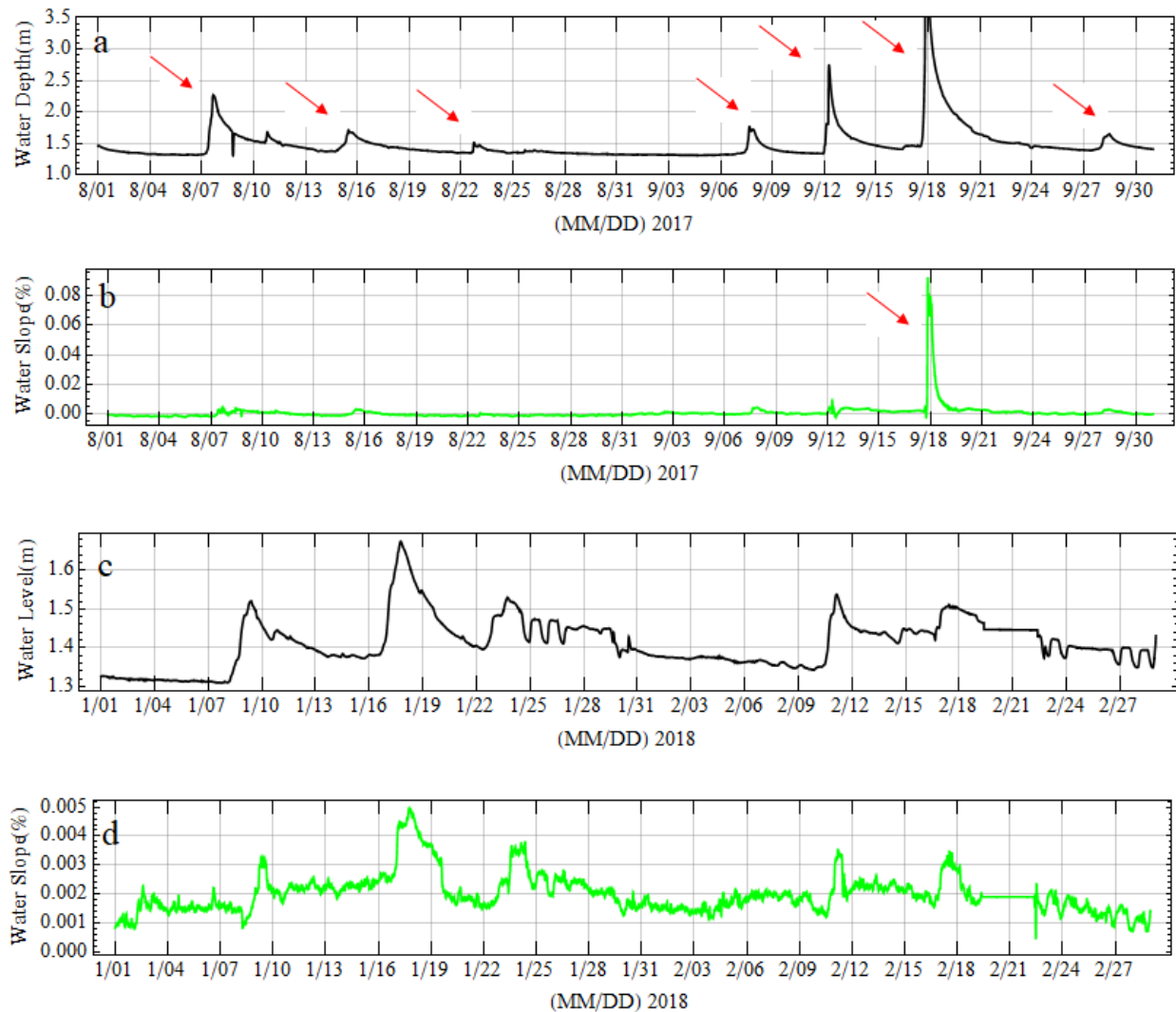
Figure 5.6 Temporal variations for water level and water surface slopes at the Basen River.
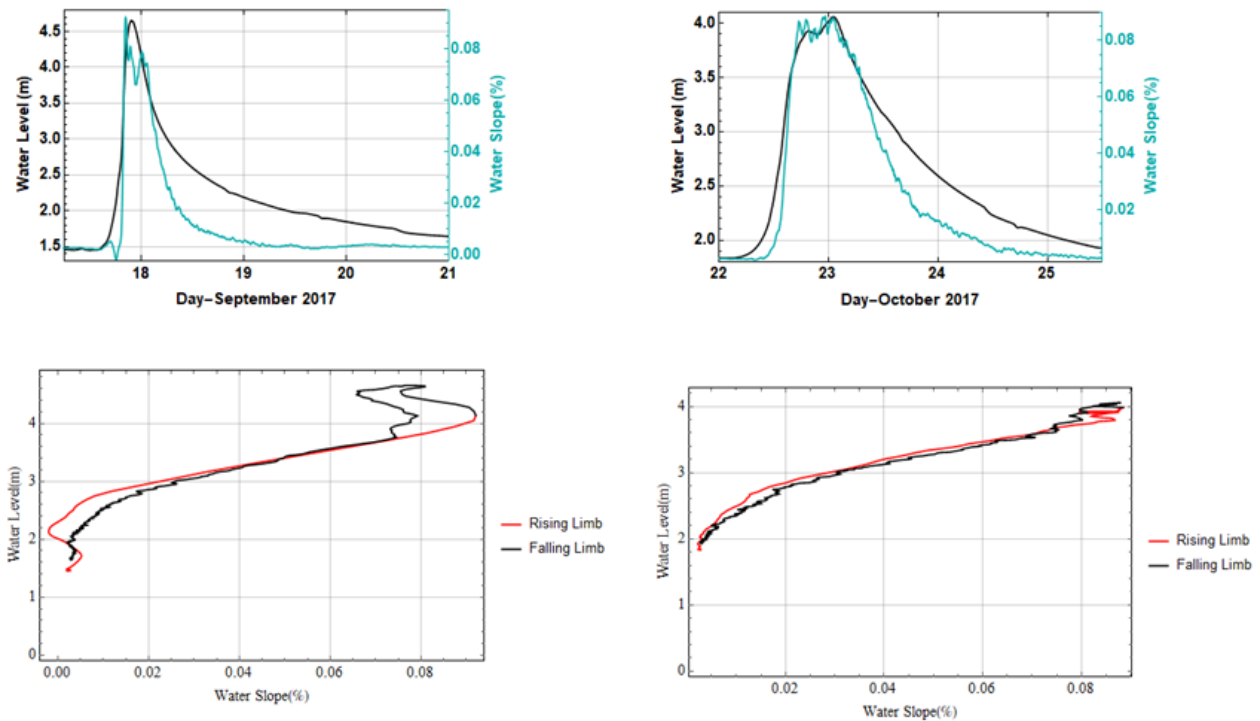
Figure 5.7 Temporal variations in water slope, corresponding (WS-WL) hysteresis for the Basen River.

5.3.5 Does the turbidity dynamics correlate with streamflow and/or water surface slope variations?

As far as it is known, there are several studies concerns about the relationships between the SSC and Q and the corresponding hysteresis patterns generated and the reason behind each form. The author already concluded that there is no direct relationship between water surface slope and the discharge variations so that it cannot be directly interpret the (Q-WL) loops by means of (WS-WL) loops. Turbidity is commonly viewed as a proxy for determining the SS content in rivers by calibrating site-specific empirical relationships between turbidity and in-situ measured sediment concentration [45]. Then the author tried to inspect if there is a potential association or connection among the different river dynamics (Q, WS, WL, Turbidity). Fig.5.8 compares the dynamics of turbidity during high intensity events. However, it was found that turbidity dynamics are independent either from water slope or streamflow variations.
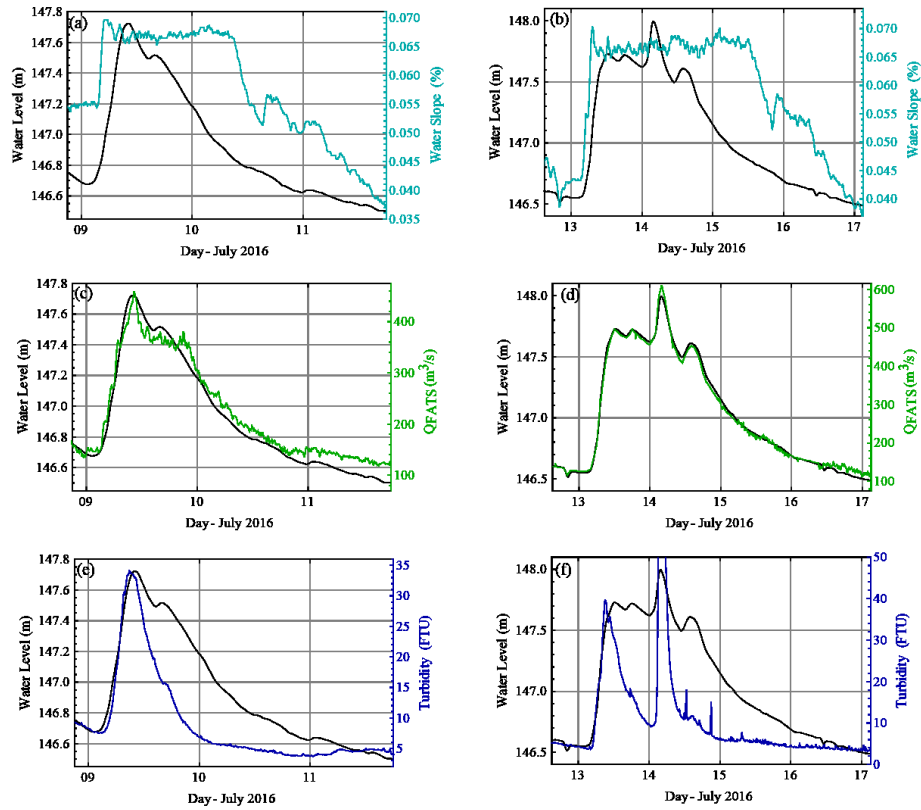
Figure 5.8 Temporal variations in water slope, temporal variations in streamflow, and temporal variation of water turbidity.

5.4 Conclusions

This chapter, a contribution toward monitoring the unsteady behavior of discharge-stage hysteresis in a mountainous river. In order to monitor the unsteady patterns of river discharge hysteresis estimated by means of a novel fluvial acoustic tomography system (FATS), the author therefore observed the corresponding river water surface slopes hysteresis during different rainfall events.

Major conclusions can be summarized as follows:

1. Temporal variations in water surface slope-stage during different scales of rainfall events forms different patterns of hysteresis loops which can be classified into three main categorize: (i) no hysteresis, (ii) clockwise hysteresis, and (iii) counterclockwise hysteresis. Similarly, streamflow-

stage hysteresis can be classified into three main categorize: (i) no hysteresis, (ii) clockwise hysteresis, and (iii) counterclockwise hysteresis.

2. River stage-discharge hysteresis is not solely match to its corresponding stage-water slope hysteresis.

3. Low rainfall events generally do not imply any hysteresis behavior. Meanwhile, for medium and high intensity rainfall events lead to either clockwise or counter clockwise (WS-WL) hysteresis patterns.

4. For medium and high intense hydrological events water slope show two peaks, the first water slope peak conveys information about the water slope-water level dynamics with "positive" or clockwise behavior. Whereas the second peak showed increasing of water slope over a certain water level.

5. For medium and high intense hydrological events, water surface slope become almost constant after passing a certain level.

6. It was noticed that for small basins water slope hysteresis cannot be documented easily, monitoring water surface slope dynamics are not informative in small basins and no clear hysteresis loops can be observed.

7. It was found that turbidity dynamics are independent either from water slope or streamflow variations.

CHAPTER 6: Conclusions and Future works

6.1 Main conclusions

The main purpose of this research is to investigate the issues subjected to long-term and high-frequency streamflow variations mainly by means of a novel hydroacoustic tomography system and comparing the new estimates to the other current and common methodologies used for continuous monitoring of discharges in unsteady shallow gravel-bed streams. Field observations of this dissertation were conducted mainly in the Gono River, which is a shallow gravel-bed river located in the city of Miyoshi, Japan.

High-frequency monitoring of river discharge variations has received a slight interest in the world. This is because the most practiced method in the world is the indirect method for estimating discharge namely; RC method. Therefore, the main contribution of this work is to improve the knowledge about the unsteady dynamics of river discharge uncertainties over high frequency scales. The measurement techniques, analysis methodologies used herein can be applied to any river of different watershed areas from small to large ones.

The specific conclusions and contributions of this study can be summarized as:

i.   Scaling characteristics of river discharge fluctuations determined by two approaches: RC since FATS. In contrast to the RC method, the results obtained by FATS are more accurate, because the discharge evaluated by FATS decomposes velocity and depth into two ratings instead of rating the stage component to discharge as done in the RC method which assumes that the river discharge in river is steady.

ii. Unlike the RC approach, FATS detected a crossover time lagged by 42 ± 21 h, which is considerable and might indicate substantial values for larger watershed. The crossover time is mainly a function of the watershed area, andthe results indicated that crossover times observed by FATS are inversely proportional with the number of peaks. That is to say, the crossover time delayed as the total time for runoff event decreased according to the runoff events and dam flush inputs.

iii.   The observed dam flush patterns of streamflow near to the Ozekiyama station by means of the FATS showed significant variation between the flushing point and the measuring station.

iv.   Fascinatingly, new phenomena were detected in this research that were not observed by the RC method, namely the presence of discharge secondary peaks (SDPs) and discharge shoulders (DSs) within DF events for discharges estimated by means of FATS. These features are linked to the unsteady behavior of the streamflow within a DF event. These phenomena may be justified due to the unsteady behavior of the river streamflow at a particular cross section is subject to spatial variations in water depth and velocity as a result of channel expansion and contraction. Furthermore, FATS can capture the river discharge-stage hysteresis, which is characterized by narrow and nested loops in the case of the Gono river.

v.   The behavior of T–Q hysteresis loops reflect the variations in channel scouring and deposition within dam flushing events. According to the sequence of peak turbidity and discharge, two types of T–Q loops were observed: counterclockwise, which was the most common type, and figure-of-eight loops.

vi.   Although it was relatively far from the dam flushing point to the observed location, the basic cause for counterclockwise hysteresis is more likely due to the soil erodibility and scouring during the flushing process across river waterway being mobilized from the great distance between the experiment site and the flushing points.

vii.   Temporal variations in water slope graphs during a single hydrological event exhibit two peaks. The first peak is subjected to the observed streamflow peak. Whereas, the second peak where observed in the falling limb and likely to be induced by the backwater effects.

viii.   Water slope-stage hysteresis patterns showed that the first water slope peak conveys information about the water slope-water level dynamics with "positive" or clockwise behavior, i.e. water level maxima precedes water slope peak. Meanwhile the second peak showed increasing of water slope over a certain water level.

ix.   Streamflow-stage hysteresis for discharges estimated by CSA method had very narrow loops increases with large-scale rainfall events. Additionally, a quasi-steady state relationship between streamflow and water level can be observed.

x.   Streamflow-stage hysteresis for discharges estimated by means of FATS approach exhibited unsteady behavior. Similarly, the hysteresis loop increases with large-scale rainfall events.

xi.   Finally, it was demonstrated that FATS has high performance in detecting the unsteady behavior of streamflow and a promising key tool for investigating various hydrological issues in the field of water resources.

6.2 Future works

The research does not stop, enormous amount of points must be investigated, however, it is suggested some additional future investigations:

- Since FATS was able to capture stage-discharge hysteresis loops clearly, it is recommended to carry out full hydrological year to examine the seasonal effect or any potential relationship between seasonality and stage-discharge hysteresis.

- Examining the temporal variations of water-slope during different scales of rainfall events, probably water slope has different behaviors over various water levels. That is to say, the in low and medium rainfall scales the water slopes is influenced by stream morphology, depth, river-bed shape. However, it is important to understand the water slope behavior and the underlying issues in the case of over bank flows.

References

[1]   V. Livina, Y. Ashkenazy, Z. Kizner, V. Strygin, A. Bunde, S. Havlin, A stochastic model of river discharge fluctuations, in: Phys. A Stat. Mech. Its Appl., 2003: pp. 283–290. doi:10.1016/j.physa.2003.08.012.

[2]   J.-H. Kang, Y.S. Lee, S.J. Ki, Y.G. Lee, S.M. Cha, K.H. Cho, J.H. Kim, Characteristics of wet and dry weather heavy metal discharges in the Yeongsan Watershed, Korea, Sci. Total Environ. 407 (2009) 3482–3493. doi:10.1016/j.scitotenv.2009.02.021.

[3]   C. V Miller, G.D. Foster, B.F. Majedi, Baseflow and stormflow metal fluxes from two small agricultural catchments in the Coastal Plain of the Chesapeake Bay Basin, United States, Appl. Geochemistry. 18 (2003) 483–501. doi:10.1016/S0883-2927(02)00103-8.

[4]   M. Peraza-Castro, S. Sauvage, J.M. Sánchez-Pérez, E. Ruiz-Romera, Effect of flood events on transport of suspended sediments, organic matter and particulate metals in a forest watershed in the Basque Country (Northern Spain), Sci. Total Environ. 569–570 (2016) 784–797. doi:10.1016/j.scitotenv.2016.06.203.

[5]   A.C. Gellis, M.K. Myers, G.B. Noe, C.R. Hupp, E.R. Schenk, L. Myers, Storms, channel changes, and a sediment budget for an urban-suburban stream, Difficult Run, Virginia, USA, Geomorphology. 278 (2017) 128–148. doi:10.1016/j.geomorph.2016.10.031.

[6]   H. Marttila, B. Kløve, Dynamics of erosion and suspended sediment transport from drained peatland forestry, J. Hydrol. 388 (2010) 414–425. doi:10.1016/j.jhydrol.2010.05.026.

[7]   K. Kawanisi, M. Razaz, K. Ishikawa, J. Yano, M. Soltaniasl, Continuous measurements of flow rate in a shallow gravel-bed river by a new acoustic system, Water Resour. Res. 48 (2012) 1–10. doi:10.1029/2012WR012064.

[8]   K. Kawanisi, M. Razaz, J. Yano, K. Ishikawa, Continuous monitoring of a dam flush in a shallow

river using two crossing ultrasonic transmission lines, Meas. Sci. Technol. 24 (2013) 055303. doi:10.1088/0957-0233/24/5/055303.

[9]   K. Kawanisi, M. Bahrainimotlagh, M.B. M.B., M. Razaz, High-frequency streamflow acquisition and bed level/flow angle estimates in a mountainous river using shallow-water acoustic tomography, Hydrol. Process. 30 (2016) 2247–2254. doi:10.1002/hyp.10796.

[10]   W. Munk, C. Wunsch, Ocean acoustic tomography: a scheme for large scale monitoring, Deep Sea Res. Part A, Oceanogr. Res. Pap. 26 (1979) 123–161. doi:10.1016/0198-0149(79)90073-6.

[11]   D. Behringer, T. Birdsall, M. Brown, B. Cornuelle, R. Heinmiller, R. Knox, K. Metzger, W. Munk, J. Spiesberger, R. Spindel, D. Webb, P. Worcester, C. Wunsch, A demonstration of ocean acoustic tomography, Nature. 299 (1982) 121–125. doi:10.1038/299121a0.

[12]   A. Kaneko, G. Yuan, N. Gohda, I. Nakano, Optimum design of the ocean acoustic tomography system for the Sea of Japan, J. Oceanogr. 50 (1994) 281–293. doi:10.1007/BF02239518.

[13]   J.-H. Park, A. Kaneko, Assimilation of coastal acoustic tomography data into a barotropic ocean model, Geophys. Res. Lett. 27 (2000) 3373–3376. doi:10.1029/2000GL011600.

[14]   M. Razaz, K. Kawanisi, A. Kaneko, I. Nistor, Application of acoustic tomography to reconstruct the horizontal flow velocity field in a shallow river, Water Resour. Res. 51 (2015) 9665–9678. doi:10.1002/2015WR017102.

[15]   A. Laenen, W. Smith., Acoustic systems for the measurement of streamflow, 1983. http://pubs.usgs.gov/wsp/2213/report.pdf.

[16]   J. V Sloat, W.S. Gain, Application of acoustic velocity meters for gaging discharge of three low-velocity tidal streams in the St. Johns River Basin, northeast Florida, (1995) iv, 26 p. file://catalog.hathitrust.org/Record/003791204.

[17]   M. Razaz, K. Kawanisi, I. Nistor, S. Sharifi, An acoustic travel time method for continuous

velocity monitoring in shallow tidal streams, Water Resour. Res. 49 (2013) 4885–4899. doi:10.1002/wrcr.20375.

[18]   K. Kawanisi, M. Bahrainimotlagh, M.B. Al Sawaf, M. Razaz, High-frequency streamflow acquisition and bed level/flow angle estimates in a mountainous river using shallow-water acoustic tomography, Hydrol. Process. 30 (2016) 2247–2254. doi:10.1002/hyp.10796.

[19]   Y. Tessier, S. Lovejoy, P. Hubert, D. Schertzer, S. Pecknold, Multifractal analysis and modeling of rainfall and river flows and scaling, causal transfer functions, J. Geophys. Res. 101 (1996) 26427.

[20]   G. Pandey, S. Lovejoy, D. Schertzer, Multifractal analysis of daily river flows including extremes for basins of five to two million square kilometres, one day to 75 years, J. Hydrol. 208 (1998) 62–81.

[21]   X. Zhou, N. Persaud, H. Wang, H. Lin, Multifractal scaling of daily runoff time series in agricultural watersheds, J. Am. Water Resour. Assoc. 42 (2006) 1659–1670.

[22]   D. Labat, A. Mangin, R. Ababou, Rainfall-runoff relations for karstic springs: Multifractal analyses, J. Hydrol. 256 (2002) 176–195.

[23]   J.W. Kantelhardt, E. Koscielny-Bunde, D. Rybski, P. Braun, A. Bunde, S. Havlin, Long-term persistence and multifractality of precipitation and river runoff records, J. Geophys. Res. Atmos. 111 (2006).

[24]   F.A. Hirpa, M. Gebremichael, T.M. Over, River flow fluctuation analysis: Effect of watershed area, Water Resour. Res. 46 (2010).

[25]   V. Livina, Z. Kizner, P. Braun, T. Molnar, A. Bunde, S. Havlin, Temporal scaling comparison of real hydrological data and model runoff records, J. Hydrol. 336 (2007) 186–198. doi:10.1016/j.jhydrol.2007.01.014.

[26]   M. Mudelsee, Long memory of rivers from spatial aggregation, Water Resour. Res. 43 (2007).

[27]   D. Labat, J. Masbou, E. Beaulieu, A. Mangin, Scaling behavior of the fluctuations in stream flow at the outlet of karstic watersheds, France, J. Hydrol. 410 (2011) 162–168.

[28]   C.K. Peng, S. V. Buldyrev, S. Havlin, M. Simons, H.E. Stanley, A.L. Goldberger, Mosaic organization of DNA nucleotides, Phys. Rev. E. 49 (1994) 1685–1689. doi:10.1103/PhysRevE.49.1685.

[29]   Z. Chen, P.C. Ivanov, K. Hu, H.E. Stanley, Effect of nonstationarities on detrended fluctuation analysis, Phys. Rev. E - Stat. Nonlinear, Soft Matter Phys. 65 (2002). doi:10.1103/PhysRevE.65.041107.

[30]   E. Koscielny-Bunde, J.W. Kantelhardt, P. Braun, A. Bunde, S. Havlin, Long-term persistence and multifractality of river runoff records: Detrended fluctuation studies, J. Hydrol. 322 (2006) 120–137. doi:10.1016/j.jhydrol.2005.03.004.

[31]   J.W. Kantelhardt, D. Rybski, S.A. Zschiegner, P. Braun, E. Koscielny-Bunde, V. Livina, S. Havlin, A. Bunde, Multifractality of river runoff and precipitation: comparison of fluctuation analysis and wavelet methods, Phys. A Stat. Mech. Its Appl. 330 (2003) 240–245. doi:10.1016/j.physa.2003.08.019.

[32]   K. Kawanisi, M. Razaz, A. Kaneko, S. Watanabe, Long-term measurement of stream flow and salinity in a tidal river by the use of the fluvial acoustic tomography system, J. Hydrol. 380 (2010) 74–81. doi:10.1016/j.jhydrol.2009.10.024.

[33]   H.M. Raghunath, Hydrology : Principles, Analysis, Design, 2nd ed., NEW AGE INTERNATIONAL (P) LIMITED, PUBLISHERS, New Delhi, 2006.

[34]   B.M. Dolgonosov, K.A. Korchagin, N. V. Kirpichnikova, Modeling of annual oscillations and 1/f-noise of daily river discharges, J. Hydrol. 357 (2008) 174–187. doi:10.1016/j.jhydrol.2008.04.023.

[35]   Kondolf, PROFILE: Hungry Water: Effects of Dams and Gravel Mining on River Channels, Environ. Manage. 21 (1997) 533–51. doi:21(4):533-51.

[36]   G.S. Bilotta, R.E. Brazier, Understanding the influence of suspended solids on water quality and aquatic biota, Water Res. 42 (2008) 2849–2861. doi:10.1016/j.watres.2008.03.018.

[37]   J.A. Sweka, K.J. Hartman, Influence of Turbidity on Brook Trout Reactive Distance and Foraging Success, Trans. Am. Fish. Soc. 130 (2001) 138–146. doi:10.1577/1548-8659(2001)130<0138:IOTOBT>2.0.CO;2.

[38]   N.E.M. Asselman, Suspended sediment dynamics in a large drainage basin: the River Rhine, Hydrol. Process. 13 (1999) 1437–1450. doi:10.1002/(SICI)1099-1085(199907)13:10<1437::AID-HYP821>3.0.CO;2-J.

[39]   P.F. Hudson, Event sequence and sediment exhaustion in the lower Panuco Basin, Mexico, CATENA. 52 (2003) 57–76. doi:10.1016/S0341-8162(02)00145-5.

[40]   X. Fan, C. Shi, W. Shao, Y. Zhou, The suspended sediment dynamics in the Inner-Mongolia reaches of the upper Yellow River, CATENA. 109 (2013) 72–82. doi:10.1016/j.catena.2013.05.010.

[41]   H.G. Smith, D. Dragovich, Interpreting sediment delivery processes using suspended sediment-discharge hysteresis patterns from nested upland catchments, south-eastern Australia, Hydrol. Process. 23 (2009) 2415–2426. doi:10.1002/hyp.7357.

[42]   V. Aich, A. Zimmermann, H. Elsenbeer, Quantification and interpretation of suspended-sediment discharge hysteresis patterns: How much data do we need?, CATENA. 122 (2014) 120–129. doi:10.1016/j.catena.2014.06.020.

[43]   J.L. Langlois, D.W. Johnson, G.R. Mehuys, Suspended sediment dynamics associated with snowmelt runoff in a small mountain stream of Lake Tahoe (Nevada), Hydrol. Process. 19 (2005)

3569–3580. doi:10.1002/hyp.5844.

[44]   D.M. Lawler, G.E. Petts, I.D.L. Foster, S. Harper, Turbidity dynamics during spring storm events in an urban headwater river system: The Upper Tame, West Midlands, UK, Sci. Total Environ. 360 (2006) 109–126. doi:10.1016/j.scitotenv.2005.08.032.

[45]   G. Göransson, M. Larson, D. Bendz, Variation in turbidity with precipitation and flow in a regulated river system – river Göta Älv, SW Sweden, Hydrol. Earth Syst. Sci. 17 (2013) 2529–2542. doi:10.5194/hess-17-2529-2013.

[46]   J. Lewis, Turbidity-Controlled Suspended Sediment Sampling for Runoff-Event Load Estimation, Water Resour. Res. 32 (1996) 2299–2310. doi:10.1029/96WR00991.

[47]   D. Pavanelli, A. Pagliarani, SW—Soil and Water, Biosyst. Eng. 83 (2002) 463–468. doi:10.1006/bioe.2002.0126.

[48]   D. Pavanelli, A. Bigi, A New Indirect Method to estimate Suspended Sediment Concentration in a River Monitoring Programme, Biosyst. Eng. 92 (2005) 513–520. doi:10.1016/j.biosystemseng.2005.08.004.

[49]   N. Diodato, Modelling net erosion responses to enviroclimatic changes recorded upon multisecular timescales, Geomorphology. 80 (2006) 164–177. doi:10.1016/j.geomorph.2006.02.007.

[50]   S. Ochiai, K. Kashiwaya, Measurement of suspended sediment for model experiments using general-purpose optical sensors, CATENA. 83 (2010) 1–6. doi:10.1016/j.catena.2010.06.008.

[51]   H. Chanson, M. Takeuchi, M. Trevethan, Using turbidity and acoustic backscatter intensity as surrogate measures of suspended sediment concentration in a small subtropical estuary, J. Environ. Manage. 88 (2008) 1406–1416. doi:10.1016/j.jenvman.2007.07.009.

[52]   A.R. Ram, J.P. Terry, Stream turbidity responses to storm events in a pristine rainforest watershed on the Coral Coast of southern Fiji, Int. J. Sediment Res. 31 (2016) 279–290.

doi:10.1016/j.ijsrc.2016.07.002.

[53]   N.I. Tananaev, M.V. Debolskiy, Turbidity observations in sediment flux studies: Examples from

Russian rivers in cold environments, Geomorphology. 218 (2014) 63–71.

doi:10.1016/j.geomorph.2013.09.031.

[54]   A.D. Ziegler, S.G. Benner, C. Tantasirin, S.H. Wood, R.A. Sutherland, R.C. Sidle, N. Jachowski,

M.A. Nullet, L.X. Xi, A. Snidvongs, T.W. Giambelluca, J.M. Fox, Turbidity-based sediment

monitoring in northern Thailand: Hysteresis, variability, and uncertainty, J. Hydrol. 519 (2014)

2020–2039. doi:10.1016/j.jhydrol.2014.09.010.

[55]   G. Di Baldassarre, A. Montanari, Uncertainty in river discharge observations: a quantitative

analysis, Hydrol. Earth Syst. Sci. 13 (2009) 913–921. doi:10.5194/hess-13-913-2009.

[56]   H. McMillan, J. Freer, F. Pappenberger, T. Krueger, M. Clark, Impacts of uncertain river flow data

on rainfall-runoff model calibration and discharge predictions, Hydrol. Process. (2010) n/a-n/a.

doi:10.1002/hyp.7587.

[57]   T.B. Ramos, M.C. Gonçalves, M.A. Branco, D. Brito, S. Rodrigues, J.-M. Sánchez-Pérez, S.

Sauvage, Â. Prazeres, J.C. Martins, M.L. Fernandes, F.P. Pires, Sediment and nutrient dynamics

during storm events in the Enxoé temporary river, southern Portugal, CATENA. 127 (2015) 177–

190. doi:10.1016/j.catena.2015.01.001.

[58]   M.B. Al Sawaf, K. Kawanisi, J. Kagami, M. Bahreinimotlagh, M.M. Danial, Scaling

characteristics of mountainous river flow fluctuations determined using a shallow-water acoustic

tomography system, Phys. A Stat. Mech. Its Appl. 484 (2017) 11–20.

doi:10.1016/j.physa.2017.04.168.

[59]   M. Bahreinimotlagh, K. Kawanisi, M.M. Danial, M.B. Al Sawaf, J. Kagami, Application of

shallow-water acoustic tomography to measure flow direction and river discharge, Flow Meas.

Instrum. 51 (2016) 30–39. doi:10.1016/j.flowmeasinst.2016.08.010.

[60]   K. Lee, A.R. Firoozfar, M. Muste, Technical Note: Monitoring of unsteady open channel flows using the continuous slope-area method, Hydrol. Earth Syst. Sci. 21 (2017) 1863–1874. doi:10.5194/hess-21-1863-2017.

[61]   and W.S.M. Smith. C F, Cordova. J T, The Continuous Slope-Area Method for Computing Event Hydrographs Scientific Investigations Report 2010-5241, (2010).

[62]   F.M. Henderson, Open channel flow, Macmillan, 1966.

[63]   G. Zuecco, D. Penna, M. Borga, H.J. van Meerveld, A versatile index to characterize hysteresis between hydrological variables at the runoff event timescale, Hydrol. Process. 30 (2016) 1449–1466. doi:10.1002/hyp.10681.

[64]   G.P. Williams, Sediment concentration versus water discharge during single hydrologic events in rivers, J. Hydrol. 111 (1989) 89–106. doi:10.1016/0022-1694(89)90254-0.

[65]   A.M. De Girolamo, G. Pappagallo, A. Lo Porto, Temporal variability of suspended sediment transport and rating curves in a Mediterranean river basin: The Celone (SE Italy), CATENA. 128 (2015) 135–143. doi:10.1016/j.catena.2014.09.020.

[66]   K. Vercruysse, R.C. Grabowski, R.J. Rickson, Suspended sediment transport dynamics in rivers: Multi-scale drivers of temporal variation, Earth-Science Rev. 166 (2017) 38–52. doi:http://dx.doi.org/10.1016/j.earscirev.2016.12.016.

[67]   P. BAČA, Hysteresis effect in suspended sediment concentration in the Rybárik basin, Slovakia / Effet d'hystérèse dans la concentration des sédiments en suspension dans le bassin versant de Rybárik (Slovaquie), Hydrol. Sci. J. 53 (2008) 224–235. doi:10.1623/hysj.53.1.224.

[68]   V.A. Levesque, K.A. Oberg, Computing Discharge Using the Index Velocity Method, 2012.

[69]   T. Dalrymple, M.A. Benson, Measurement of peak discharge by the slope-area method, 1968.
         http://pubs.er.usgs.gov/publication/twri03A2.

[70]   K. a. Moller, O. Fryd, a. De Neergaard, J. Magid, Economic, environmental and socio-cultural
         sustainability of three constructed wetlands in Thailand, Environ. Urban. (2012).
         doi:10.1177/0956247811434259.

[71]   A.M. Stewart, J.B. Callegary, C.F. Smith, H. V. Gupta, J.M. Leenhouts, R.A. Fritzinger, Use of
         the continuous slope-area method to estimate runoff in a network of ephemeral channels, southeast
         Arizona, USA, J. Hydrol. (2012). doi:10.1016/j.jhydrol.2012.09.022.

[72]   K. Kawanisi, M.B. Al Sawaf, M.M. Danial, Automated Real-Time Streamflow Acquisition in a
         Mountainous River Using Acoustic Tomography, J. Hydrol. Eng. 23 (2018) 04017059.
         doi:10.1061/(ASCE)HE.1943-5584.0001604.

[73]   S.E. Rantz, Measurement and Computation of Streamflow, Vol. 1 - Meas. Stage Discharge, USGS
         Water Supply Pap. 2175. (1982). doi:10.1029/WR017i001p00131.

[74]   M. Muste, H.-C. Ho, D. Kim, Considerations on direct stream flow measurements using video
         imagery: Outlook and research needs, J. Hydro-Environment Res. 5 (2011) 289–300.
         doi:10.1016/j.jher.2010.11.002.

[75]   A.R. Schmidt, Analysis of Stage-Discharge Relations for Open -Channel Flows and Their
         Associated Uncertainties, University of Illinois at Urbana-Champaign, 2002.
         doi:http://hdl.handle.net/2142/83191.